# Pulsed Laser Deposition: Fundamentals, Applications, and Perspectives

Floriana Craciun, Thomas Lippert, and Maria Dinescu

## Contents



**Abstract**

Pulsed laser deposition (PLD) has established itself as one of the pillar techniques for the growth of thin films and nanostructures. The fundamental aspects and applications of PLD described in this chapter do not aim to offer an exhaustive view about this field of science, but rather to describe a brief evolution of its conceptual background in order to settle on the most prominent state-of-the-art

F. Craciun
Istituto di Struttura della Materia-CNR (ISM-CNR), Area della Ricerca di Roma-Tor Vergata, Rome, Italy
e-mail: floriana.craciun@isc.cnr.it

T. Lippert
Research with Neutrons and Muons Division, Paul Scherrer Institute, Villigen, Switzerland

Department of Chemistry and Applied Biosciences, Laboratory of Inorganic Chemistry, ETH Zurich, Zurich, Switzerland
e-mail: thomas.lippert@psi.ch

M. Dinescu (✉)
National Institute for Laser, Plasma and Radiation Physics, Magurele, Romania
e-mail: dinescum@ifin.nipne.ro



K. Sugioka (ed.), *Handbook of Laser Micro- and Nano-Engineering*,
https://doi.org/10.1007/978-3-319-69537-2_27-1

achievements. The fundamental discussion around the technique emphasizes how initial efforts to achieve a comprehensive picture that relates target laser ablation to plasma kinetics and to thin film growth were critical in understanding the overwhelming complexity of the relationship between these processes and experimental parameters, such as laser pulse properties, type of vacuum or ambient atmosphere, substrate characteristics, and others. With these in mind, state-of-the-art thin films grown by PLD came to rely on an ab initio design of interfacial characteristics that was achieved by correlating their underlying physical interactions to experimental conditions. This approach has yielded remarkable results, particularly for multicomponent thin films, in view of next-generation applications in ferroelectrics and multiferroics, superlattices, photocatalysis, photovoltaics, etc. The perspectives of PLD in relation to the latest developments in the field are also discussed.

## Introduction

Pulsed laser deposition (PLD) is a physical vapor deposition technique that relies on the interaction between a high-power pulsed laser beam and the surface of a target material, which in most cases is a solid. The area onto which the laser beam is focused undergoes several transformations that involve heating, melting, and/or local vaporization of the material, provided that the laser fluence exceeds a certain threshold particular to every type of material. PLD experiments are usually carried out either in vacuum or low-pressure gas atmosphere, and as a result the material that is vaporized from the target following laser interaction forms a characteristic plasma plume, which expands symmetrically with respect to an axis perpendicular to the surface of the target (Fig. 1).

The purpose of this general approach that PLD enables, and which can have many particularities depending on the selected experimental environment, is in fact to transform a solid material into a reactive collection of its constituents and to favorably manipulate them toward achieving thin films or nanostructures that display properties or even novel functionalities, inaccessible in the bulk state. To this end, in the simplest of approaches, the ablated material is collected on a substrate placed parallel to the target. The composition of the deposited film can be the same as that of the target or different, depending on the presence of a reactive gas that can be introduced in the deposition chamber. The film can be amorphous or crystalline, with preferential orientation determined by various parameters like substrate type and temperature, gas pressure, laser fluence, substrate-target distance, etc. Since the first PLD paper published by Smith and Turner in 1965 (Smith and Turner 1965), the field expanded, facing issues and fulfilling requirements, such as those related to droplet removal, reproducibility, and large-area scaling up.

The PLD technique itself is simple and versatile, but due to the fact that it involves a large number of experimental parameters affecting both the ablation and thin film growth processes, it is also difficult to master. Nevertheless, the

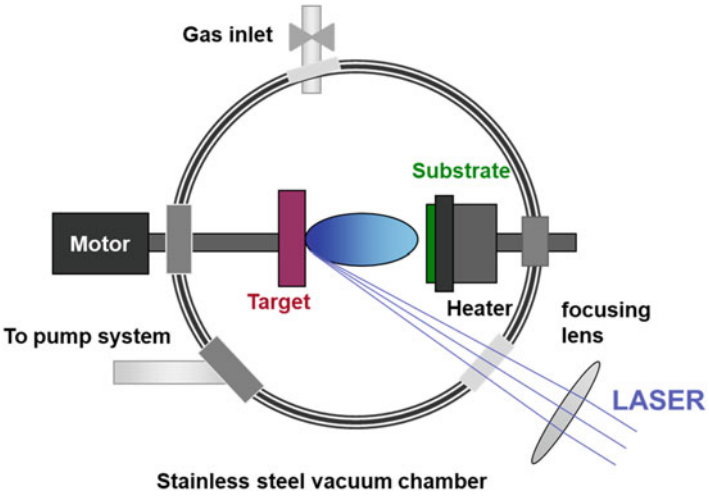


**Fig. 1** General PLD setup

technique has seen a rapid adoption by the materials science community because of its many advantages with respect to other growth methods (Chrisey and Hubler 1994; Bäuerle 2011; Eason 2007), such as the following:

(i) It allows the synthesis of metastable phases that cannot by produced by "standard" techniques.
(ii) The possibility, in specific experimental conditions, of transferring complicated stoichiometries from bulk into thin film, as in the case of superconductors having high critical temperature ($T_C$), piezoelectric and ferroelectric compounds, biocompatible materials (hydroxyapatite), etc.
(iii) The laser source is external to the reaction chamber, which makes it a "clean" reactor.
(iv) The laser beam is incident on a small zone on the target surface, which results in high efficiency, control, and flexibility of the process.
(v) No charge effects appear.
(vi) No "memory" reactor, i.e., the possibility to deposit heterostructures by changing the target and/or the reactive gas as well.
(vii) Compounds having different compositions than the target can be obtained through a single step process: synthesis and deposition (GaN from Ga in $N_2$ (Dinescu et al. 1998), ZnO from Zn in $O_2$ (Dinescu and Verardi 1996; Verardi et al. 1996, 1999), $Si_3N_4$ from Si in $NH_3$ (Studenikin et al. 1998)).
(viii) It allows the decrease of the deposition temperature, and, very often, no subsequent thermal treatments are required (Craciun et al. 2002).

The different stages of the PLD process have been intensively studied: (i) laser-target interaction (coupling, heat equation, phase transitions, depending both on

target and laser characteristics, etc.), (ii) plasma expansion in vacuum or in gases (collisions, cluster formation), and (iii) film growth. Numerous papers and books/book chapters were published, and different models of laser-matter interaction in pulsed laser deposition have been proposed.

Perhaps the first comprehensive attempt at achieving a complete modeling of the PLD process that relates the laser ablation step to the plasma plume expansion, and subsequently to the thin film growth, is the study by Rajiv K. Singh and J. Narayan (1990). This study evidenced the sheer complexity of the PLD technique, in spite of its apparent simplicity. The relationship between process parameters such as laser fluence, wavelength, pulse duration, target material characteristics, and target to substrate distance were demonstrated to have a critical impact on plasma plume dynamics and thin film properties. The study assumed a statistical model for the particular case of nanosecond laser pulses using an excimer laser source, as well as several other approximations.

The subsequent study by Anisimov et al. (1993) improved on the model of Rajiv K. Singh and J. Narayan by also considering spatial temperature gradients in the plasma plume, which had been neglected in the previous study, and by assuming an adiabatic expansion of the plume. The model allowed for the estimation of ablated species temperature (kinetic energy) when reaching the substrate, which is of interest toward achieving a control over the resulting thin film epitaxy.

Finally, another milestone study by A. Miotello and R. Kelly (1995) focused on the laser-target interaction to reveal that the problem was much more complex than previously thought and that the heating/evaporation of the target is a result of several competing processes, which can be of thermal, electronic, or sputtering nature, depending both on the laser pulse (e.g., pulse length, fluence, wavelength) and target characteristics. The major breakthrough of this study was the understanding that thermal processes were dominant in the case of *ns* laser pulses, whereas electronic contributions would be an advantage of *fs* laser sources, which would allow the decreasing of the ablation threshold by one to two orders of magnitude. In spite of this advantage, and although there has been a continuous adoption of *fs* sources for materials processing by pulsed laser ablation, the use of *ns* laser pulsed sources, and excimer lasers in particular, continues to yield the best results in the field of PLD (Scarisoreanu et al. 2017) and to be the de facto choice of most groups, likely due to their reduced cost and ease of operation with respect to their *fs* counterparts.

As the field of PLD expanded and diversified into the twenty-first century, it became clear that the statistical models proposed initially were having an increasingly difficult time in describing ablation processes of targets that would not fit the ideal approximations assumed in those models. As a result, many groups trying to gain a deeper fundamental insight on laser-target interaction and thin film growth processes resorted to more complex approaches that involve either the use of Monte Carlo atomistic simulations for the description of melting, ablation, and solidification of targets following laser interaction (Lorazo et al. 2006) or the use of kinetic models that are adapted to the peculiar growth characteristics of a material of interest (Puretzky et al. 2014), rather than using broad models with oversimplifying approximations. The current trends for material processing using the PLD technique have

capitalized on these new insights by inspiring researchers to use a "bottom-up" approach in designing their experiments around critical aspects of thin film growth, such as plasma expansion (Ojeda-G-P et al. 2018), nucleation, growth kinetics, substrate-induced interactions, strain effects, etc. (Ossi 2018).

In the next section, the following discussion on the state of the art of PLD applications is based on the very premise that novel functionalities can indeed be obtained using this technique through the realization of multicomponent thin films and heterostructures. However, this can be achieved only by taking advantage of both intrinsic particle kinetics characteristic to the pulsed laser ablation process and their interaction with specifically tailored substrate and/or buffer systems. As a consequence, unique functional characteristics can result from the heavily modified interfacial arrangements, stemming from a favorable interplay between experimental process parameters and advanced materials design concepts, such as strain engineering, self-assembly, superlattices, etc.

## Applications of PLD

### Ferroelectric Thin Films

Ferroelectric materials and thin films have been intensively investigated in the last decades, owing to a combination of dielectric and electromechanical properties with a wide spectrum of applications. While new or improved properties have been generally achieved by compositional modifications, in the last years, the availability of sophisticated techniques for film deposition boosted the field of property modification by **strain engineering**. Generally, strain engineering of **ferroelectric thin films** is based on selecting a substrate with adequate mismatch, which, however, allows only a limited range of lattice deformation owing to the lattice relaxation above the critical thickness. The requirement for integration with silicon wafers is another limiting factor. These limitations imposed the necessity to employ techniques which allow growing epitaxial strained films with larger thicknesses on various substrates. In the PLD technique, one has the possibility to vary many growth parameters, among which the most important are the gas pressure and the substrate temperature. For example, a recent research (Lyu et al. 2018) demonstrated how to grow epitaxial ferroelectric thin films on silicon with larger thicknesses and strain levels. **$BaTiO_3$ (BTO) films** have been deposited on Si (001) substrates buffered with yttria-stabilized zirconia (YSZ), $CeO_2$, and $LaNiO_2$ (LNO). The BTO/LNO/$CeO_2$/YSZ heterostructures were deposited in sequence on Si(001) substrates by PLD, with a KrF excimer laser with a repetition frequency 5 Hz. The BTO films were deposited at 700 °C under dynamic oxygen pressure ($pO_2$) of 5 $10^{-3}$, 0.01, 0.015, 0.02, 0.05, and 0.1 mbar. The key parameter is the oxygen pressure, which is used to modulate the energy of the laser-generated plasma. At low values of oxygen pressure, the plasma ions are more energetic and create point defects. Thus, the amount of defects and oxygen vacancies is higher at lower oxygen pressure and influences the film structure by favoring the expansion of the unit cell. Since the

BTO film is clamped on the substrate, it expands along the out-of-plane direction, thus growing with polar axis orientation along this direction. Conversely, films grown at higher oxygen pressure are a-oriented. It has been demonstrated that the tetragonality of the films is controlled by the oxygen pressure. With this procedure BTO films with thicknesses >100 nm, high strain levels (>0.8%) and selected polar axis orientation (either parallel or perpendicular to the substrate surface plane) have been obtained. Thus, the oxygen pressure parameter can be used to control both strain and texture of the grown films, demonstrating to be an effective unconventional strain engineering tool (Lyu et al. 2018).

Technological demands impose also other types of substrates for the growth of ferroelectric and **piezoelectric thin films**. For example, for applications such as adaptive X-ray optics devices for telescopes, interferometry space satellite applications, transparent touch panels, etc., highly efficient piezoelectric thin films such as **$Pb(Zr,Ti)O_3$** must be grown on transparent ultralow expansion glass substrates. Nguyen et al. have demonstrated that by using **$Ca_2Nb_3O_{10}$ (CNO) nanosheet layers** deposited on ultralow expansion glass substrates as seed layers, PZT films with preferential (001) orientation can be grown by PLD by using a KrF excimer laser source (the laser repetition frequency is 10–50 Hz with an energy density of 2.5 J/cm$^2$, substrate temperature of 600 °C, and oxygen pressure of 0.1 mbar) (Nguyen et al. 2017b). The thickness of the CNO nanosheet is a few nm. Moreover, it has been found that also deposition parameters such as the laser repetition frequency and substrate temperature are important for the microstructure and electrical properties. Thus a columnar grain structure has been obtained for films deposited with high repetition frequency. Due to this columnar structure which allows the [001] preferential alignment, an enhanced $d_{33}$ piezoelectric longitudinal coefficient of 356 pm/V was measured on PZT/CNO/glass heterostructure (PZT film thickness of 2 μm). In Fig. 2a, b AFM images of the film surface and SEM images on cross section are displayed. It can be observed that the surface is uniform and that the columnar structure of PZT film on LNO/CNO/glass extends over the whole thickness.

The important role of the CNO nanosheet in favoring film texture is shown in Fig. 3 where the polarization and piezoelectric properties of PZT films on different substrates (LNO/glass, TiO/glass, and CNO/glass) are displayed. The PZT films have been deposited at 50 Hz and 600 °C. The piezoelectric constant value for the PZT film deposited on CNO/glass was found to be higher, confirming that the growth on seeding layers such as CNO is a valid strategy for obtaining high-quality ferroelectric and piezoelectric films.

In search of ferroelectric materials for next-generation ferroelectric memories, the attention has been focused also on **conductive domain walls** that could be in principle used for nondestructive electrical readout of the polarization states. Recently, Jiang et al. used specific domain wall configurations in epitaxial $BiFeO_3$ (BFO) thin films grown on (001) $SrTiO_3$ (STO) substrates by PLD to demonstrate nondestructive readout of stored states (Jiang et al. 2018).

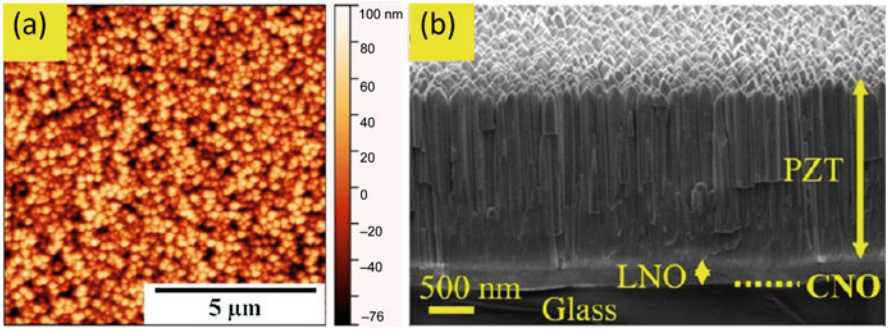


**Fig. 2** (**a**) AFM image of PZT film deposited on CNO/glass substrate; (**b**) SEM image on cross section (Nguyen et al. 2017b)

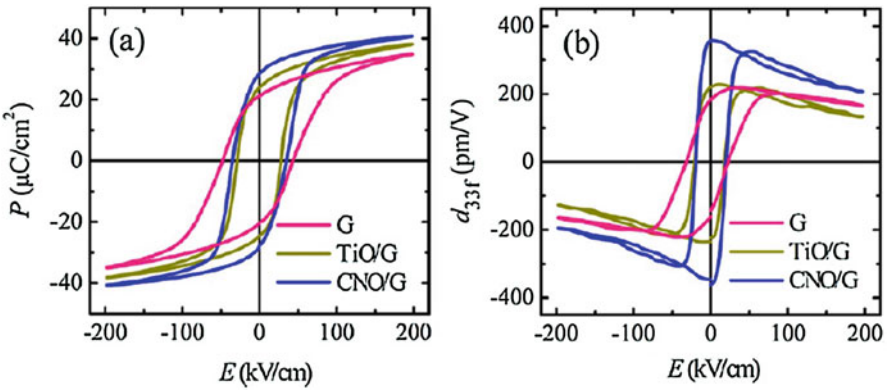


**Fig. 3** (**a**) Polarization, electric field hysteresis loops for PZT films deposited on different substrates; (**b**) piezoelectric constant, electric field hysteresis loops (Nguyen et al. 2017b)

Domain wall conduction has been investigated also in other thin films deposited by PLD, like tetragonal (001)-oriented $Pb(Zr_{0.1}Ti_{0.9})O_3$ thin films with a thickness of 70 nm grown on (001)STO substrates (McGilly et al. 2015).

Thus, research carried out in the last years allowed to foresee the possible active role of ferroelectric domain walls in nanoelectronics. It has been demonstrated, for example, that the conductivity of the domain walls can be modulated as a function of domain wall curvature (Vasudevan et al. 2012). Indeed, the charge formed at the interface results into the movement of carriers or vacancies for neutralization. This has been demonstrated by ultrahigh vacuum scanning probe microscopy (SPM) measurements on $BiFeO_3/SrRuO_3$(SRO) heterostructures grown by PLD on $DyScO_3$ (DSO) substrates.

Other promising candidates for nonvolatile resistive memories are **ferroelectric tunnel junctions** (FTJ) formed by two metal electrodes separated by an ultrathin ferroelectric barrier. By switching the polarization in the ferroelectric

barrier, the barrier height seen by electrons can be set to a high or low value, which gives rise to a **tunneling electroresistance (TER)**.

Further attempts to develop better FTJ devices resulted into new asymmetric tunneling heterostructures with one of the metallic electrodes substituted by a heavily doped semiconductor (Wen et al. 2013). A FTJ based on Pt/BaTiO3/Nb:$SrTiO_3$ heterostructure has been proposed. The semiconductor substrate was a (001)-oriented single crystal of 0.7% Nb-doped $SrTiO_3$ (Nb:STO) on which a BTO ultrathin film with a thickness of 7 unit cells (u.c) (controlled by RHEED) was deposited. The BTO film was epitaxially grown layer by layer by PLD with a KrF laser by applying 2.5 J/cm$^2$ laser energy density, a repetition rate of 2 Hz, substrate temperature of 750 °C, and an oxygen pressure of $5*10^{-3}$ mbar. In the new FTJ based on metal/FE/semiconductor heterostructure, the modulation of the height barrier is accompanied also by a space charge region produced by the ferroelectric field. The nonvolatile resistance switching in Pt/BTO/Nb:STO is displayed in Fig. 4a, where a huge ON/OFF ratio $> 10^4$ is registered. The retention properties are shown in Fig. 4b, where the resistance contrast within 24 h remains almost unvaried. These characteristics indicate a potential of the proposed devices for nondestructive readout **nonvolatile memories.**

Other results regarding enhanced TER in tunneling junctions based on ferroelectrics or multiferroics grown by PLD have been reported in Refs. (Yin et al. 2013; Li et al. 2014; Gajek et al. 2007).

The importance of ferroelectric domains and domain walls as control tools for novel devices has been recently revealed. The growth of ferroelectric epitaxial films with controllable domain configurations is therefore highly praised. Agar et al. have recently demonstrated the influence of compositional and strain gradients on the domain structure of PZT films (Agar et al. 2016). For this, two heterostructures (thickness 100 nm), one with homogeneous composition $Pb(Zr_{0.2}Ti_{0.8})O_3$ and another one compositionally graded ($Pb(Zr_{0.2}Ti_{0.8})O_3$ on bottom and $Pb(Zr_{0.8}Ti_{0.2})O_3$ on top, have been grown by PLD on SRO/$GdScO_3$ (110) substrates. The compositional gradients have been employed in order to obtain an increase of the in-plane lattice parameter along the film thickness. The compositionally graded PZT layers were grown by using a programmable target rotator correlated with the excimer laser, at 600 °C in an oxygen pressure of 200 mTorr. The ferroelectric domain structure imaged by piezoresponse force microscopy (PFM) is shown in Fig. 5 for both homogeneous and compositionally graded heterostructures. The presence of compositional and strain gradients stabilizes the tetragonal phase in the compositionally graded heterostructure, although its top composition is rhombohedral.

In the search for new materials for ferroelectric memories, **strain engineering** has been applied to different oxide films grown by PLD, in order to induce or enhance ferroelectric properties. Thus it has been pointed out that epitaxial hafnia-based thin films can show an enhanced ferroelectricity when grown with ultrathin thickness, thus being very promising for future memory devices. For this high-quality epitaxial films must be grown. Recently Wei et al. reported the epitaxial growth of $Hf_{0.5}Zr_{0.5}O_2$ (HZO) thin films with thicknesses in the range of 1.5–27 nm (Wei et al. 2018). HZO films were grown on (001)-oriented

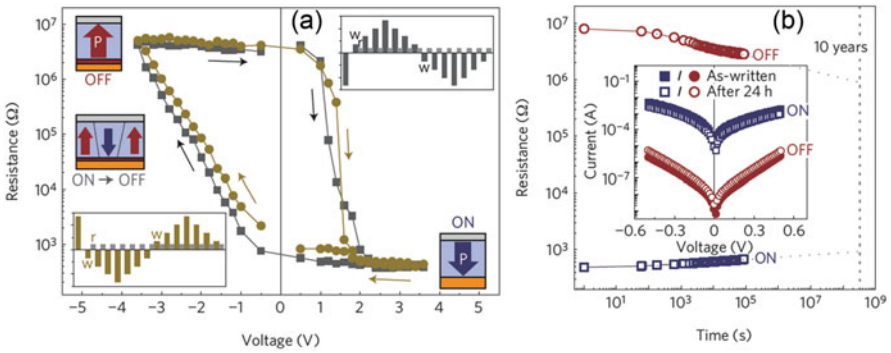


**Fig. 4** (**a**) Tunneling electroresistance hysteresis loop of Pt/BTO/Nb:STO FTJ. In the insets the corresponding domain evolution is schematically shown. (**b**) Retention properties. The inset shows the current-voltage curves before and after measurements are shown in the inset (Wen et al. 2013)

$La_{0.7}Sr_{0.3}MnO_3$(LSMO)/$SrTiO_3$ substrates by PLD. The substrate temperature was 800 °C and the oxygen pressure was 0.1 mbar. Under epitaxial compressive strain, the HZO films show ferroelectric polarization values of about 34 μC/cm$^2$.

Strain engineering has been used also to enhance the Curie temperature ($T_c$) of $BaTiO_3$ from 130 °C (bulk value) to 330 °C for a thin film, by using a special growth PLD process which results into self-assembling vertical columns of $Sm_2O_3$ throughout the film thickness (Harrington et al. 2011). The $Sm_2O_3$ columns (10 nm in diameter) grow in the BTO matrix and induce a strain of 2.35%. The BTO matrix is thus forced to preserve its tetragonal structure due to **lateral straining**. Thus a very high transition temperature is obtained. One must mention that enhancement of $T_c$ in thin films is usually obtained by using conventional substrate-induced epitaxial strain. However, because of strain relaxation through the thickness, only very thin films can be grown. This limitation is not favorable for those applications which require thicker films. Instead the new method proposed by Harington et al. seems adequate for strain control in thicker films being based on the growth of **vertical nanocomposites**. The strong increase in $T_c$ from 130 °C to 330 °C has been demonstrated in a film with thickness larger than 1.2 μm. Films were grown by PLD on (001) Nb-doped STO substrates at 800 °C in 0.2 mbar of oxygen from a target of 0.5 BTO-0.5 SMO.

Figure 6 shows a TEM image taken on the cross section of a film with a thickness of 600 nm. Self-assembled SmO nanocolumns (diameter 10 nm) are clearly visible in the BTO matrix of the composite film. The nanocolumns extend in the direction perpendicular to the substrate through the whole film thickness. The growth process of SMO nanocolumns inside the BTO matrix is controlled by the minimization of the composite surface energy. In this nanostructure the lower compliance phase (the BTO matrix) adapts to accommodate the mismatch strain with the higher compliance phase (the SMO nanocolumns) and therefore becomes strained (+2.35% out-of-plane). Different combinations of hard/soft phases can be

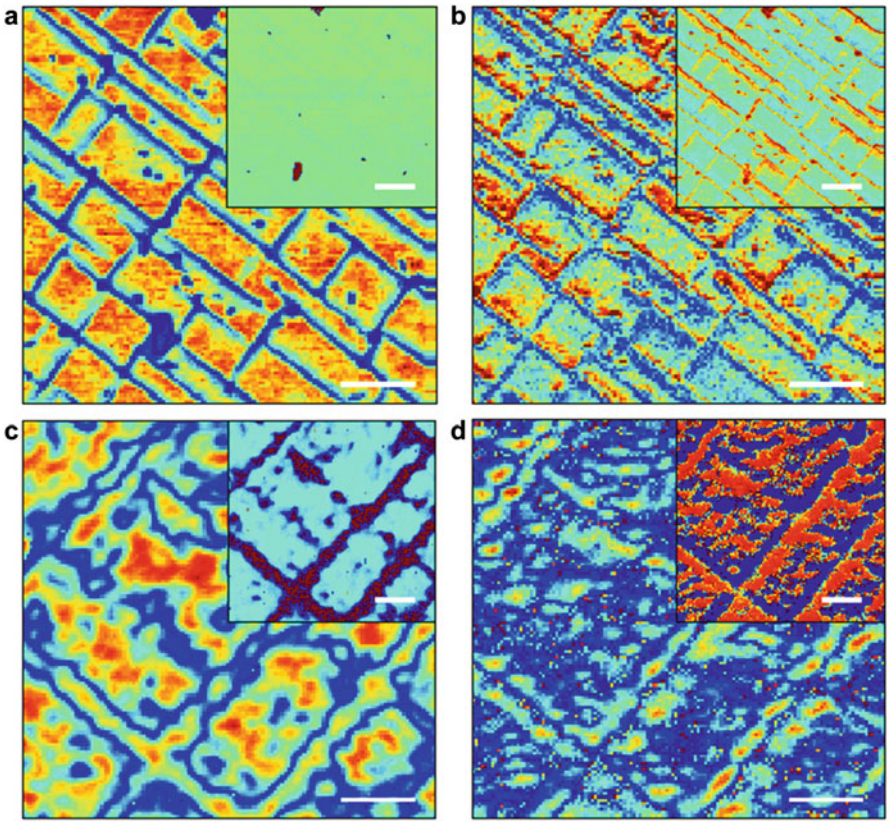


**Fig. 5** (**a**, **b**) PFM images (vertical and lateral amplitudes) of domain structures in homogeneous $Pb(Zr_{0.2}Ti_{0.8})O_3$ heterostructure; (**c**, **d**) PFM images (vertical and lateral amplitudes) of domain structures in compositionally graded heterostructures (Agar et al. 2016)

imagined thus, allowing an **effective strain tailoring** inside films with thicknesses well above the conventional film thickness.

Ferroelectric hysteresis measurements confirmed the existence of ferroelectricity to at least 330 °C in a composite film with a thickness of 1 μm (Fig. 7). A remnant polarization $P_r$ of about 21 μC/cm$^2$ was registered at room temperature and, remarkably, at 330 °C, thus proving that the strain coupling between the BTO matrix and the SMO nanocolumns is effective in preventing strain relaxation along the film thickness. This is confirmed also by the dielectric constant vs. temperature curves, shown in the upper inset. The sharp dielectric peak at 700 °C signals the tetragonal-cubic phase transition. Although ferroelectric hysteresis loops for temperatures >330 °C are not shown, eventually the composite film could be ferroelectric also at higher temperatures. The lower inset shows that also leakage current properties have been improved with respect to a pure BTO film, showing that the leakage current was reduced with respect to a pure BTO film. On the whole these results

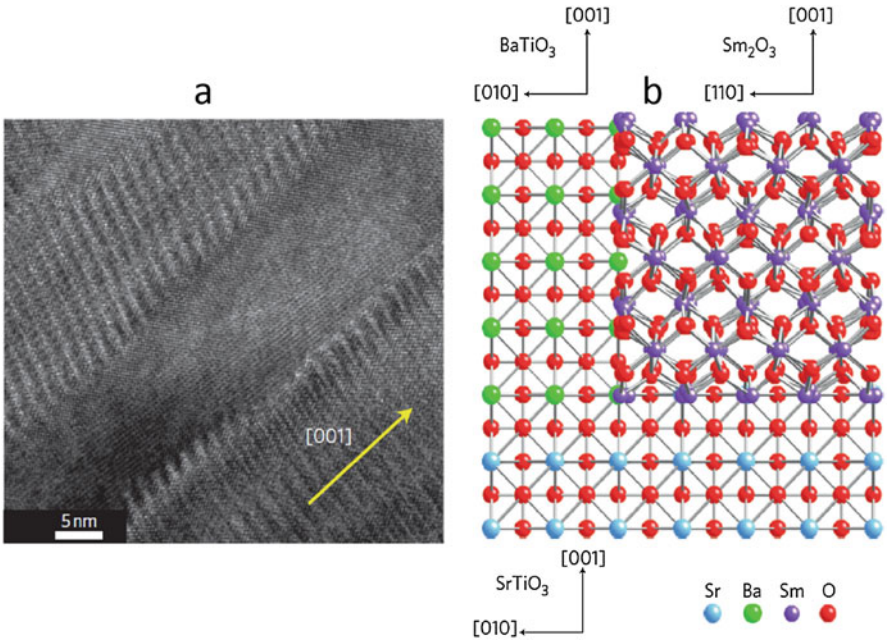


**Fig. 6** (**a**) Cross section TEM image of a self-assembled vertical nanostructure of $BaTiO_3$:$Sm_2O_3$ on $SrTiO_3$. The yellow arrow represents the c-axis direction; (**b**) proposed model for interface matching in BTO-SMO thin films (Harrington et al. 2011)

indicate that BTO-SMO **self-assembled nanoscale composites** deposited by PLD are tetragonal and potentially ferroelectric up to 700 °C, opening the way to high-temperature nanoscale ferroelectrics.

Highly oriented lead-free multilayered BaTiO3-(Ba,Ca)$TiO_3$-$CaTiO_3$ thin films were fabricated on (001) Nb:STO substrates by PLD with enhanced dielectric and tunability performance (Zhu et al. 2016)

Epitaxial **lead-free ferroelectric thin films** of (Ba,Ca)(Zr,Ti)O3 deposited by PLD on various substrates with enhanced dielectric and piezoelectric properties have been reported in Refs (Scarisoreanu et al. 2015; Ion et al. 2018).

$Pb(Zr_{0.52}Ti_{0.48})O_3$ (PZT) thin films with (001) orientation were deposited on Pt (111)/Ti/$SiO_2$/Si(100) substrates using PLD (Nguyen et al. 2017a). A strong variation of film microstructure with the **laser pulse frequency** was found. Thus, films deposited at lower pulse frequencies show a denser **columnar microstructure**. An improved effective **transverse piezoelectric coefficient** $d_{31}$ is measured on these films. Conversely, films deposited at higher pulse frequency have a less densely packed columnar microstructure which is found to enhance the **longitudinal piezoelectric coefficient** $d_{33}$. The microstructure dependence on laser pulse frequency has been rationalized in terms of diffusion time of the mobile ions on the constructing surface during deposition, while the piezoelectric coefficient dependence was attributed to the different clamping effect on the lattice in the individual grains when these

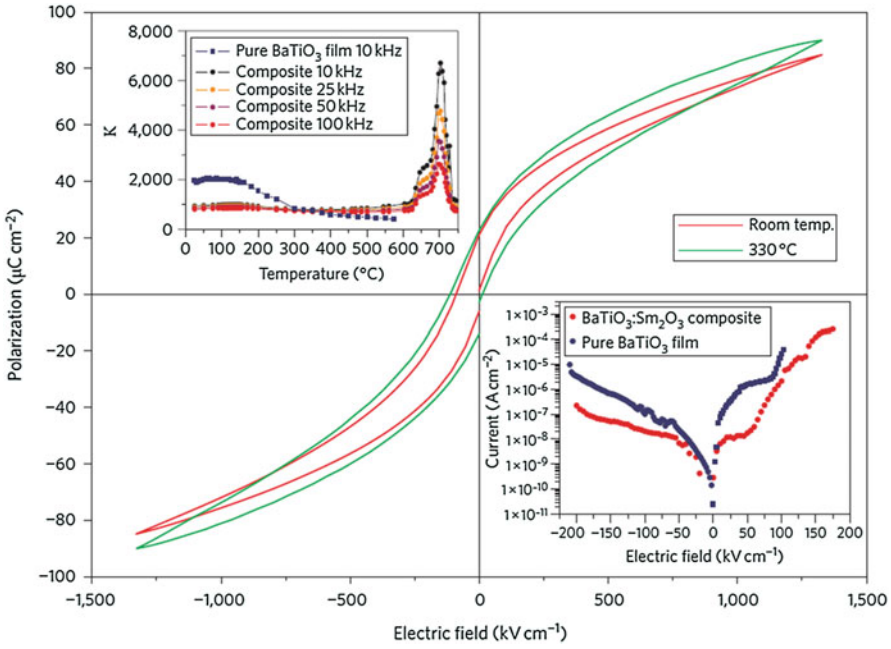


**Fig. 7** P-E hysteresis loops measured on a nanocomposite film of BTO-SmO. Upper inset: dielectric constant versus temperature pure and composite films measured at various frequencies. Lower inset: leakage current versus applied field (Harrington et al. 2011)

are more or less connected. Enhanced $d_{33}$ piezoelectric coefficients (e.g., 408 pm/V for a PZT film with thickness 4 μm) have been measured.

$BiFeO_3$ (BFO) ferroelectric thin films doped with rare-earth (RE) ions (RE = Sm, Gd, Dy) have been deposited by PLD, and the effect of different chemical pressures on the crystalline structure has been investigated (Kan et al. 2010). Pure BFO is rhombohedral (R) at ambient temperature. It has been found that all the compositions have a transition to an orthorhombic (O) paraelectric phase, showing maximization of electromechanical and dielectric properties at the phase boundary. It has been also observed that the structural transition is controlled by the average radius of the A-site cation, which changes with the type and the amount of RE substituent, indicating that the chemical pressure induced by the dopant plays the key role in structure transformation. RE-doped BFO thin films with a thickness of 400 nm were grown on different substrates: (001) $(LaAlO_3)0.3$-$(SrAl_{0.5}\ Ta_{0.5}\ O_3)0.7$ (LSAT), (001) $SrTiO_3$ (STO), and $(110)_o$ $DyScO_3$ (DSO) by PLD with an KrF excimer laser, at a temperature of 590 °C and oxygen pressure of 25 mTorr. For 12%Sm-doped BFO films dielectric constant, piezoelectric $d_{33}$ constant, and polarization values of 250, 110 pm/V, and 70 μC/cm$^2$ have been reported, respectively (Kan et al. 2010).

Also, other **RE-doped BFO thin films** have been grown by PLD (Scarisoreanu et al. 2016). The RE ion was $Y^{3+}$, and the films were grown epitaxially on (100) STO substrates, with thicknesses below 100 nm, in order to preserve the strained

condition. Under the chemical strain imposed by $Y^{3+}$ substitution and the epitaxial strain imposed by the substrate, the grown films gained a nanodomain structure favored both by the morphotropic boundary between the R and O phases (as in other RE-doped BFO films (Kan et al. 2010)) and by the partial local strain relaxation induced by the presence of defects. Owing to this nanostructure, the dielectric properties were strongly enhanced, reaching a value of about 2500 with small dielectric loss ($\tan \delta < 0.01$) for $Bi_{0.95}Y_{0.05}FeO_3$ epitaxially grown at 700 °C under 13 Pa oxygen partial pressure, by using an ArF excimer laser ($\lambda = 193$ nm) with pulse frequency of 5 Hz.

Besides controlling ferroelectricity in thin films by controlling epitaxial strain, it has been demonstrated also by Tyunina et al. that 3D film growth during hetero-epitaxy can be used to control the domain configurations (Tyunina et al. 2013). The formation of a columnar structure during film growth, observed also in Ref. (Harrington et al. 2011), although induced there by different factors, is found to be responsible for enhanced dielectric and ferroelectric properties in $Pb_{0.5}Sr_{0.5}TiO_3$ films grown epitaxially on $La_{0.5}Sr_{0.5}CoO_3$ (LSCO)/MgO (001) substrates by PLD.

Epitaxial ferroelectric thin films of $Pb(Zr_{0.2}Ti_{0.8})O_3$ deposited by PLD have been also reported in other studies (Xu et al. 2015). These films with 150 nm thickness have been grown on $SrRuO_3$ (SRO) or $La_{0.7}Sr_{0.3}MnO_3$ (LSMO)/$SrTiO_3$ (001). The polarization switching process has been investigated.

Thin films of relaxor ferroelectrics, namely, $Pb(Mg_{1/3}Nb_{2/3})O_3$-$PbTiO_3$ (PMN-PT), have been deposited by PLD for pyroelectric energy conversion and thermal energy harvesting applications (Pandya et al. 2018).

## Multiferroics

In multiferroic materials, either ferromagnetism, ferroelectricity, or ferroelasticity coexist. In a small class of materials, magnetism and ferroelectricity are coupled, giving rise to magnetoelectricity. Ferroelectric ferromagnetics are very rare, since their specific properties arise from incompatible characteristics, namely, the first have filled bands and are insulators, whereas the second have partially filled bands and are conductive. The search for room temperature multiferroics and multiferroic thin films was boosted by their promising applications, including tunable multi-functional spintronic devices, spin filters, magnetoelectric random access memory, multifunctional sensors, etc. At the same time, new physical phenomena at artificially constructed heterointerfaces, including magnetism at the interface between otherwise insulating materials, emerged as a new field for tailoring materials with exotic properties. Therefore, PLD research focused recently on such materials and phenomena.

Controlling the magnetic state of the materials by an electric field instead of a magnetic field is one of the key issues pursued in multiferroics research, with the aim to obtain electrically controllable spintronic devices. Wu et al. demonstrated the growth of high-quality multiferroic BFO thin films and ferromagnetic $La_{0.7}Sr_{0.3}MnO_3$ (LSMO) thin films by PLD, which have been employed to construct

a **field-effect device** (FED) for the electrical control of **exchange bias** (Wu et al. 2010). To build this electric FED, a thin film heterostructure of LSMO and BFO was heteroepitaxially grown by pulsed laser deposition on a STO (100) substrate. The BFO film was used as the dielectric and the ferromagnetic LSMO film as the conducting channel. Previous to the deposition, the STO substrate was prepared with a $TiO_2$-terminated atomically flat top surface, by chemical etching and thermal annealing. LSMO and BFO layers were epitaxially grown at laser energy densities of 1–1.5 J/cm$^2$ with repetition rates of 3 Hz or 1 Hz, respectively, at a substrate temperature of 700 °C in oxygen atmospheres (200 mtorr for LSMO and 100 mtorr for BFO). A post-growth annealing in an oxygen atmosphere at 760 torr while the samples cooled down to ambient temperature was performed. For employing as conducting channel in the FED, the LSMO was chosen to be 3–5 nm, in order to enhance the exchange bias and its effects at the interface. The BFO layer was chosen to be 600 nm thick, to avoid gate leakage. The effect of BFO polarization on exchange bias in LSMO layer has been characterized in the BFO/LSMO field-effect device. The exchange bias in the LSMO layer was measured for the voltage pulse sequence shown in Fig. 8a. The pulse sequence alternates between the two ferroelectric polarization states after every five pulses. The results of the electric field induced changes in the exchange bias are shown in Fig. 8b, c. As it can be observed, the exchange bias $H_{eb}$ is modulated by the application of an electric field. To reach this effect, a very high quality of the STO/LSMO interface must be achieved.

Sometimes new multiferroic materials are discovered but their phases can be metastable. This was the case for $Sr_{1-x}Ba_xMnO_3$, which in the metastable perovskite phase can show a ferroelectric state. Fortunately, this metastable phase can be stabilized in thin films, as revealed by Langenberg et al., which showed that in $Sr_{1-x}Ba_xMnO_3$ (SBMO) ($0.2 \leq x \leq 0.5$) epitaxial strained thin films, grown by PLD under optimized conditions onto various (001)-oriented perovskite substrates, the perovskite phase is fully stabilized over the nonferroelectric hexagonal phase (Langenberg et al. 2015). In such structures, a polar state, driven by a new mechanism consisting in off-centering of the non-$d_0$ $Mn^{4+}$ magnetic cation, leads to ferroelectric ordering above room temperature and high polarization values. This ferroelectric state coexists with the G-type antiferromagnetic (AFM) state arising from Mn-O-Mn superexchange interactions. Moreover, since the same ion ($Mn^{4+}$) is responsible for both ferroelectric and magnetic orders, strong magnetoelectric coupling is expected. $Sr_{1-x}Ba_xMnO_3$ ($0.2 \leq x \leq 0.5$) thin films were grown by PLD on various perovskite monocrystalline substrates (001)-oriented: $YAlO_3$ (YAO), LAO, STO, $DyScO_3$ (DSO), $TbScO_3$ (TSO), $GdScO_3$ (GSO), etc. The laser fluence and repetition rate were set to 1 J/cm$^2$ and 10 Hz, respectively. The growth process has been done at 700–1000 °C and various oxygen pressure values. After deposition the films were cooled down at 10 C/min in pure oxygen atmosphere (700 torr).

Figure 9 shows that SBMO film grown on TSO is pure pseudocubic with no secondary phase. A very high quality of the interface is observed (Langenberg et al. 2015).

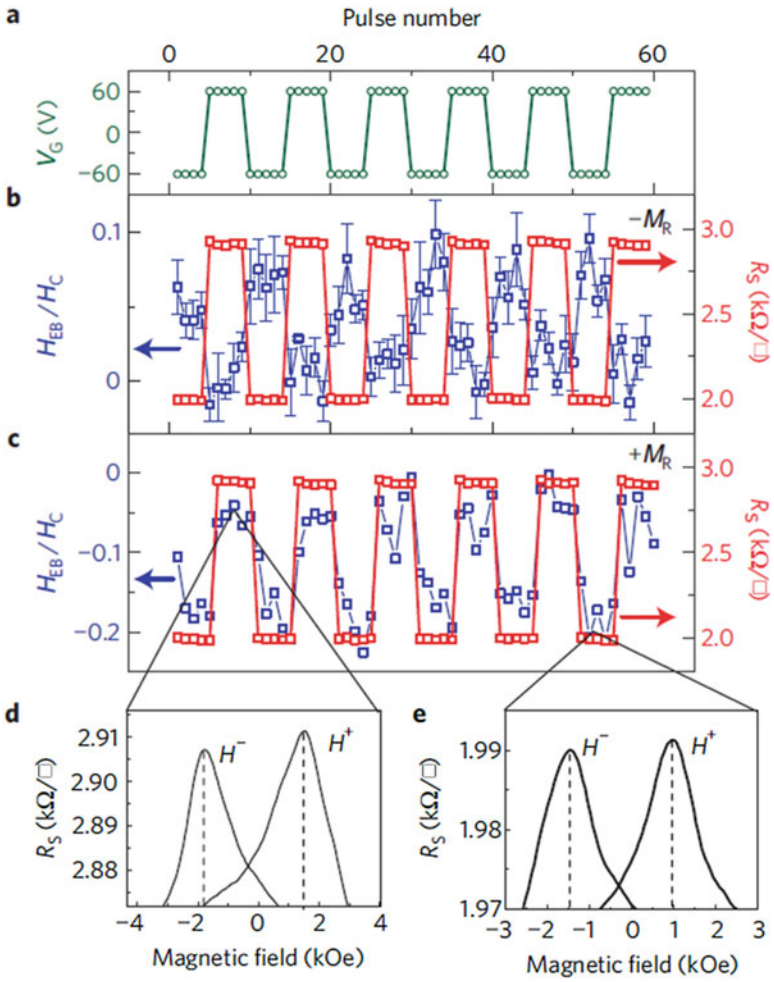


**Fig. 8** (**a**) The sequence of gate voltage pulses applied for measurements of exchange bias. (**b**) The exchange bias response to this sequence, (**c**) peak resistance, (**d**, **e**) magnetoresistance curves from the upper and lower resistive states (Wu et al. 2010)

Most of the magnetoelectric materials are composites, showing a magnetoelectric which is mediated by the elastic coupling. Typically, ferroelectric BFO and ferromagnetic $CoFe_2O_4$ (CFO) are assembled together in various proportions and geometries (connectivities) to obtain composites with magnetoelectric effect. In the last decades, composite films with different phase connectivities have been obtained. In recent years a novel BFO-CFO composite thin film with so-called **quasi (0-3) type connectivity** has been proposed in Ref. (Li et al. 2016). The composite thin films have been grown epitaxially on (110)SRO/(110)STO substrates by PLD with a laser energy density of 3 J/cm$^2$ and frequency of 1 Hz, in an oxygen pressure of 90 mTorr.

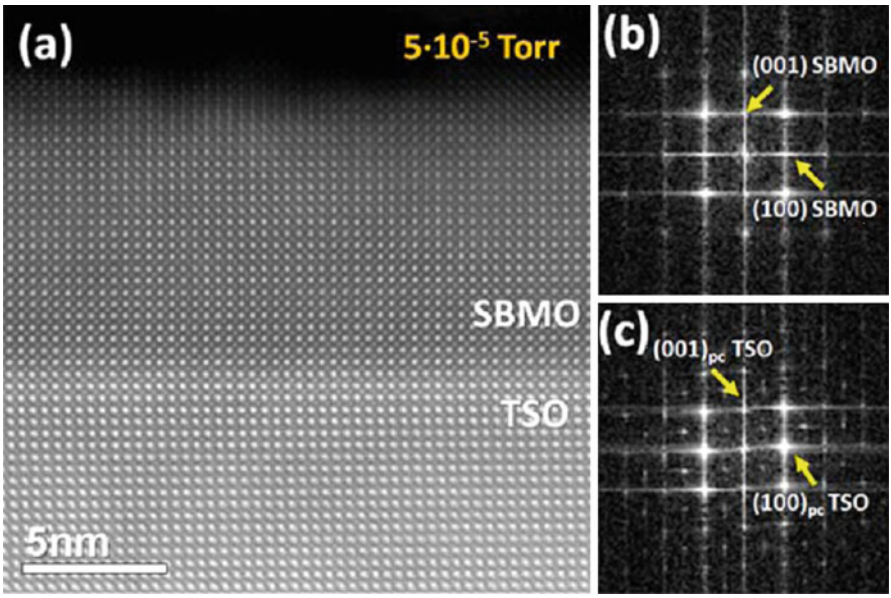


**Fig. 9** (**a**) HAADF-STEM image of [100] cross section of $Sr_{0.6}Ba_{0.4}MnO_3$ films grown at 5 $10^{-5}$ torr on the (100) $TbScO_3$ substrate, (**b**) fast Fourier transform of the film, (**c**) fast Fourier transform of the substrate

The deposition process for the growth of composite films is based on a fast switching dual-target PLD technique, where two single-phase targets of BFO and CFO have been employed. The laser beam is first focused on the CFO target and after 500 pulses is switched to the BFO target for another 500 pulses. This procedure is repeated until the final desired thickness is achieved. Although usually this procedure leads to (2-2) type films, in this case the two targets are switched at a very high frequency, and the time is sufficient to allow the full covering of the substrate, thus preventing layer-by-layer growth. In this way a (0-3) type growth is employed (Li et al. 2016). This allowed obtaining heteroepitaxial **self-assembled thin films** with quasi (0-3) nanostructures. A key parameter for obtaining the desired nanostructure and connectivity was the wetting ability of the component phases. Different wetting abilities of these BFO and CFO phases induce different growth types for the two components during the deposition process: a layer-by-layer growth for BFO and an island growth for CFO. In this progressive process, the BFO matrix interrupts the connectivity of the CFO phase. Therefore, CFO grains grow on the BFO rather than on SRO. The **magnetoelectric effect** of the ferroelectric grains and ferromagnetic grains was detected by piezoresponse amplitude mapping without and under external magnetic field. Magnetic field-induced ferroelectric switching has been observed in situ by PFM. The local ferroelectric domain evolution under external magnetic field demonstrates the strain-mediated ME coupling effect in composite multiferroics. Moreover, in the (0-3) connected composite heterostructures, the leakage current

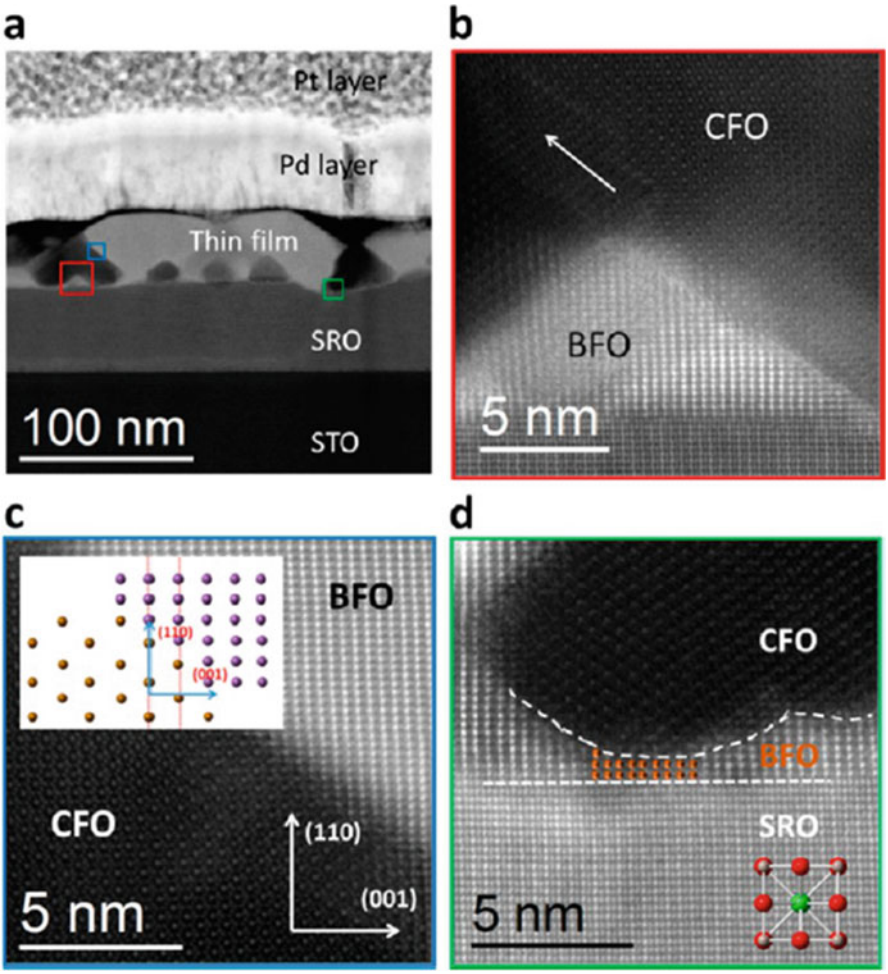


**Fig. 10** (**a**) A cross section image of the BFO-CFO composite film sandwiched between the SRO bottom and Pt top layers, (**b**–**d**) high magnification HAADF images of selected squares in (**a**) (Li et al. 2016)

was reduced as compared to other (1-3) connected structures (Li et al. 2016). The self-assembly growth mechanism has been imaged by spherical aberration corrected TEM with high-angle annular dark-field (HAADF) detector (Fig. 10a). HAADF contrast is proportional to $Z^2$ ($Z$ = atomic number); thus the dark regions in the image are CFO-rich and the bright areas are rich in BFO. The islands of CFO located inside the BFO matrix are clearly visible. Figures 10b–d show different shapes of interfaces. As shown in Fig. 10c, a well-ordered epitaxial interface with atomic resolution reveals the relationship between the BFO (110) and CFO (220) planes. An island of CFO is clearly seen with atomic resolution in Fig. 10d) (Li et al. 2016).

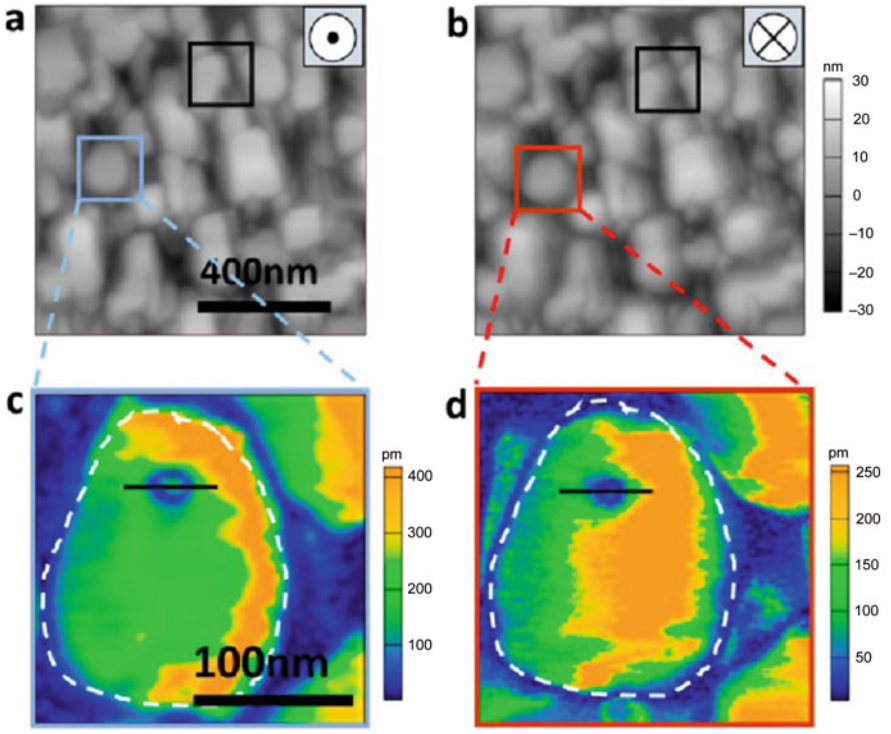


**Fig. 11** Local PFM images evidencing the action of an applied magnetic field of 9 kGauss on the motion of ferroelectric domain walls. In (**a**) and (**b**), morphology of the scanned area and in (**c**) and (**d**) PFM images after application of the magnetic field and its reversal (Li et al. 2016)

Figure 11 shows PFM images of the local magnetoelectric effect in the **nanocomposite films**. The direction of the applied magnetic field modulates the motion of the ferroelectric domains as it can be observed in panels (c) and (d). Direct observation of ferroelectric domain wall motion under external magnetic fields is an evidence for a strong ME coupling effect, revealing the potential of CFO-BFO composite films for multiferroic domain wall devices.

Multiferroic $0.85BiTi_{0.1}Fe_{0.8}Mg_{0.1}O_3$–$0.15CaTiO_3$ (BTFM-CTO) thin films have been deposited on $Pt/TiO_2/SiO_2/Si$ substrates by PLD with a laser source at 355 nm and a repetition rate of 10 Hz (Jia et al. 2018). The thin films were deposited at 500 °C, followed by an in situ thermal annealing process for 10 min. Both ferroelectric and magnetic properties have been registered at room temperature. The multifield coupling in the film has been obtained by scanning force microscopy (SFM). The switching action of magnetic and electrical fields over the ferroelectric and magnetic domains has been visualized, evidencing the existing magnetoelectric coupling (Jia et al. 2018)

Multiferroic rare-earth (R) manganites $RMnO_3$ are of great interest for applications, since they show intrinsic coupling between the ferroelectric and magnetic

order. TbMnO3 (TMO) is one of these multiferroics, which shows a high magnetoelectric coupling, but also antiferromagnetic (AFM) order; therefore it is not useful for memory devices. It has been reported (Hu et al. 2015) that this drawback can be overcome by strain and domain engineering which allow to obtain ferromagnetic TMO films. Epitaxial TMO thin films with a thickness t = 270 nm were grown on (001) Nb-doped $SrTiO_3$ (NSTO) single crystal substrates using PLD, with a KrF excimer laser with an energy density of 1 J/cm$^2$. Multiferroic $TbMnO_3$ thin films with pure c-orientation have been grown. The films possess magnetically driven multiferroicity (Hu et al. 2015).

Highly strained films of $BiFe_{0.5}Mn_{0.5}O_3$ (BFMO) grown at very low rates by PLD were demonstrated to exhibit both ferrimagnetism and ferroelectricity at RT and above (Choi et al. 2014). It has been shown that the ferrimagnetism arises from the AFM coupled $Fe^{3+}$ and $Mn^{3+}$. STEM studies showed that there was no long-range ordering of Fe and Mn. The magnetic properties were found to be strongly dependent on the strain state in the films.

Films were grown on (001) STO and (001) Nb:STO substrates by PLD with a KrF laser at 640 °C and 100 mTorr oxygen pressure.

Multiferroic epitaxial heterostructures with outstanding results grown by PLD have been also reported in other works (Eerenstein et al. 2007; Balke et al. 2009; Chu et al. 2008; Sando et al. 2013).

## Superlattices

In the last years, new phases have been explored in materials with restricted geometries such as superlattices, nanodots, nanocomposites, etc. In the case of **ferroelectric superlattices** (FE SL), the competition between electrostatic and strain boundary conditions favors the occurrence of new phases such as polarization vortices which can coexist with the ferroelectric ground state. For the deposition of FE SL, the modern PLD techniques rival by now with the traditional molecular beam epitaxy (MBE) technique. Recently $(PbTiO_3)_n/(SrTiO_3)_n$ superlattices (n = 4,6,...16) were grown on 5 nm $SrRuO_3$-buffered $DyScO_3$ (110) substrates by reflection high-energy electron diffraction (RHEED)-assisted PLD (Damodaran et al. 2017). Superlattice depositions were performed at a laser energy density of 1.5 J/cm$^2$ and at a substrate temperature of 630 °C in a dynamic oxygen pressure of 100 mTorr. An on-axis geometry was used, since it demonstrated to favor the stoichiometric transfer from the target to the substrate. The in situ RHEED monitoring growth evidenced the layer-by-layer growth during the deposition process. SLs with different periodicities and a total thickness of 100 nm have been obtained. After deposition the samples were cooled in 50 torr oxygen to room temperature to promote oxidation (Damodaran et al. 2017). Phase field models have been used to visualize how the ferroelectric phase evolves into the vortex phase (Fig. 12a). The ferroelectric phase possesses a uniform polarization along the [110] pseudocubic (pc) direction, represented by the white arrow in Fig. 12a. As one enters into the vortex phase, the polarization evolves into vortices with axes aligned along

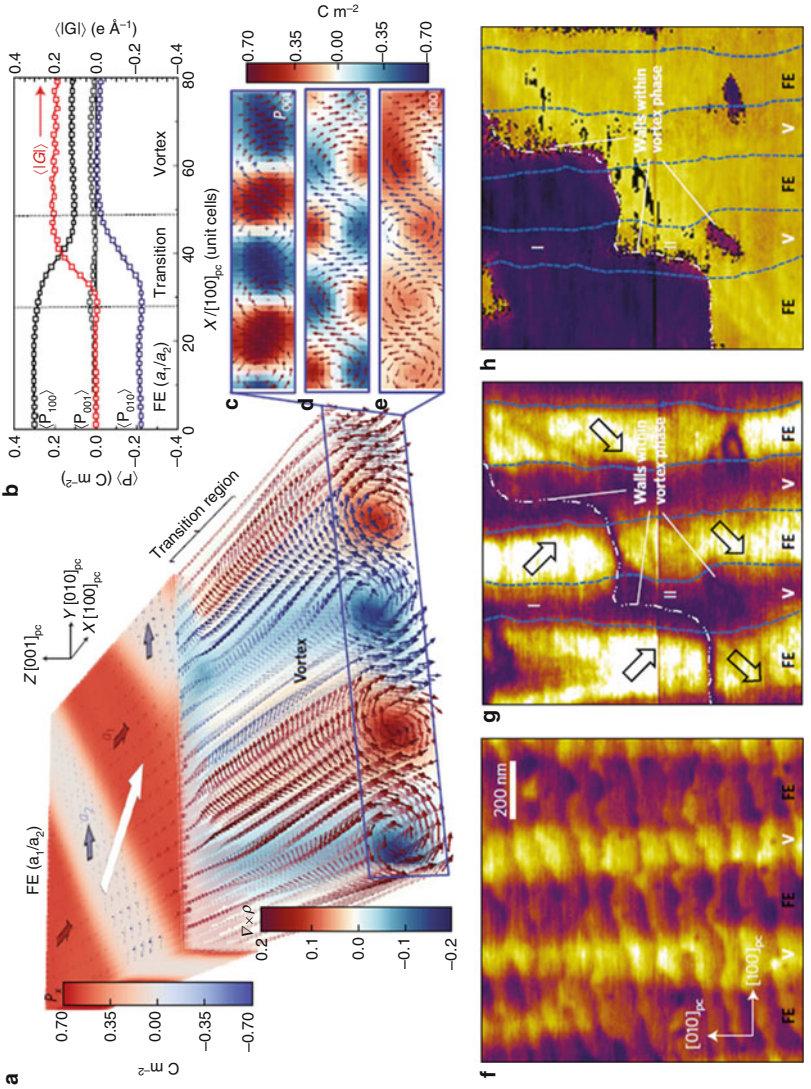


**Fig. 12** (continued)

the $[100]_{pc}$. Alternating clockwise and anticlockwise vortices are observed. The transition to the vortex phase occurs over about 20 unit cells and is characterized by complex polarization rotation pathways. PFM lateral piezoresponse force studies evidenced the presence of domain wall-like features within the vortex phase that are indicative of axial polarization components. (Fig. 12f–h). Thus phase field models and PFM data suggest that the vortex structures possess an axial component of polarization that is correlated with the polarization in the surrounding ferroelectric phase (Damodaran et al. 2017).

BTO/PZT superlattices were grown by PLD on (100)-oriented Nb:$SrTiO_3$ (NSTO) substrates using a KrF excimer laser at a wavelength of 248 nm (He and Wang 2016). First a $La_{0.7}Ca_{0.3}MnO_3$ (LCMO) epitaxial film with a thickness of 4 nm was deposited as a buffer layer to prevent polarization loss and leakage current. Then a 5 nm PZT layer was deposited on the top of the LCMO layer to reduce the lattice mismatching between the BTO and LCMO layers. Next a BTO layer with the same thickness was grown. Both BTO and PZT layers were grown at the same temperature, i.e., 650 °C, in oxygen atmosphere under 5 Pa, by alternating the BTO and PZT layers for 19 periods. Top Au electrodes with an area of about 0.2 $mm^2$ were fabricated by sputtering (He and Wang 2016). XRD measurements probed that the **BTO/PZT superlattices** were epitaxially grown on the NSTO substrates. TEM and XRD probed that high-quality ferroelectric superlattices have been grown by pulsed laser deposition. In addition, it has been found that the total thickness was about 190 nm and the individual thickness is about 48 Å. The thickness of one modulation period is therefore about 96 Å. Moreover, the authors could show that the BTO and PZT layers have grown epitaxially on each other with sharp interfaces. The epitaxial relationship between the BTO and PZT layers was also confirmed by the fast Fourier transform (FFT) patterns, and the leakage current density has been reduced by 2–3 orders of magnitude compared with both pure BTO and PZT films. This has been attributed to the role of interfaces in attracting and accumulating defects, especially oxygen vacancies, as probed by the existence of $Ti^{3+}$ ions at the interfaces, revealed by X-ray photoelectron spectroscopy (XPS). Moreover, the charges injected from the electrodes may be scattered by the sharp BTO/PZT interface, and the carrier mobility in the FE SL will be decreased (He and Wang 2016).

However, the distribution of defects influences also the ferroelectric properties. It has been found that the values of saturation and remnant polarization are smaller for the FE SL than for the individual layers (He and Wang 2016). This decreasing has been attributed to the polarization mismatch between the two layers which induces internal fields and to the existence of defect charges accumulated at the BTO/PZT interfaces.

**Fig. 12** (**a**) Phase field calculation on a single $PbTiO_3$ layer near the phase boundary, revealing a smooth transition of the ferroelectric domain to the vortex phase; (**b**) spatially averaged ferroelectric polarization components and the axial electrical toroidal moment across the phase boundary from the ferroelectric to the vortex phase; (**c**–**e**) the spatial distribution of the polarization components; (**f**–**h**) lateral piezoresponse force studies showing (**f**) topography, (**g**) lateral amplitude, and (**h**) lateral phase (Damodaran et al. 2017)

Transition metal oxide (TMO) interfaces have attracted strong interest in the last years, due to the prospects to engineer new materials by controlling and designing their electronic properties. For this aim, detailed experimental information on the orbital polarization is essential and ultimately requires very high-quality interfaces. Again, PLD demonstrated to be a reliable technique for this purpose. For example, a (4 u.c.//4 u.c.) × 8 LNO-LAO superlattice composed of the paramagnetic metal $LaNiO_3$ (LNO) and the band insulator $LaAlO_3$ (LAO) has been grown on an atomically flat single-crystal STO substrate (u.c. = pseudo-cubic unit cell) with [001] orientation by PLD using a KrF excimer laser with 2 Hz pulse repetition rate and 1.6 J/cm$^2$ energy density (Benckiser et al. 2011). Both compounds were deposited in 0.5 mbar oxygen atmosphere at 730 °C and subsequently annealed in 1 bar oxygen atmosphere at 690 °C for 30 min. As the lattice constant of cubic STO is larger than the pseudocubic lattice constants of LNO and LAO (mismatch 2%), the superlattice should be under tensile strain. The superlattice structure and interface quality were verified by high-resolution hard XRD. It was found that the strain was partially relaxed. The roughness of the interface was smaller than 1 u.c. It has been found that the 4 u.c.-thick LNO layer stacks in TMO superlattices are metallic and paramagnetic (Benckiser et al. 2011).

The impact of dynamical electron-phonon interaction on the electronic properties of artificially layered heterostructures has been investigated in high-quality YBCO-LCMO superlattices grown by PLD on $SrTiO_3$ substrates with (001) orientation (Driza et al. 2012). In this configuration the c-axis of YBCO is out of plane. The superconducting and ferromagnetic transition temperatures were measured using a vibrating sample magnetometer and superconducting quantum interference device (SQUID). It has been demonstrated that epitaxial superlattices offer opportunities to generate vibrational modes that do not exist in the bulk and control the electron-phonon interaction in transition-metal oxides at ambient pressure and without introducing chemical disorder (Driza et al. 2012).

Significant progress has been achieved also in fabricating high-quality thin film iron-based superconductors, in the form of artificially layered **pnictide superlattices**, which offer the possibility to explore superconductivity mechanisms and to tailor the superconducting properties. Moreover, the development of superconducting devices such as tunnel junctions requires multilayered heterostructures. High-quality artificially engineered undoped Ba-122/Co-doped Ba-122 compositionally modulated superlattices have been successfully grown by PLD (Lee et al. 2013a). Moreover, a structurally modulated STO/Co-doped Ba-122 superlattice with sharp interfaces has been also demonstrated. (1.2 nm STO or 3 nm O-Ba-122/13 nm and 20 nm Co-doped Ba-122)x n superlattice thin films were grown on STO-templated (001)-oriented LSAT single-crystal substrates using a KrF excimer laser in a vacuum of 3 × $10^{-4}$ Pa at 730–750 °C. The magnetization of the films was measured with a vibrating sample magnetometer at 4.2 K.

To investigate the microstructure of STO and O-Ba-122 SLs, TEM was used. Fig. 13a, b shows cross-section low- and high-magnification HAADF images of the STO SL. In Fig. 13a the bright and dark layers correspond to 13 nm Co-doped Ba-122 and 1.2 nm STO layers, respectively. The image illustrates that there are 24 STO/Co-

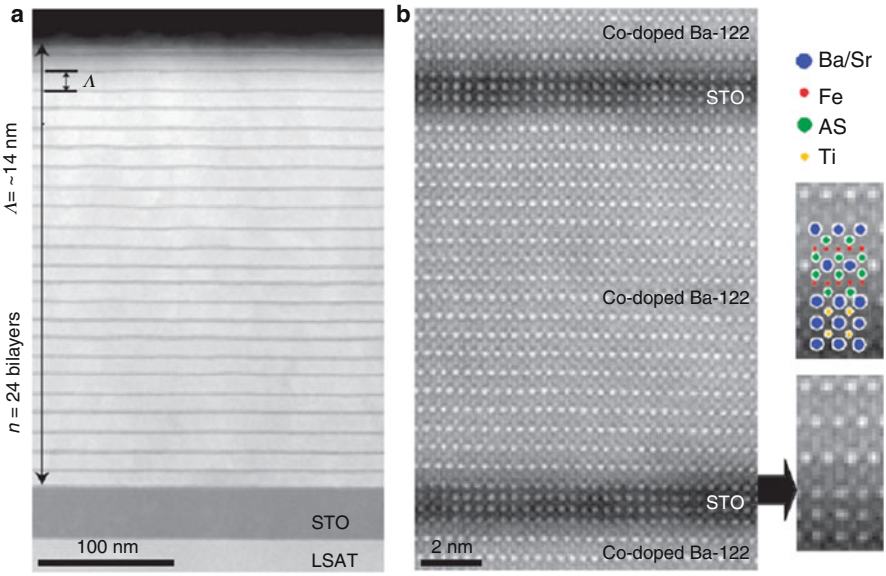


**Fig. 13** (**a**, **b**) HAADF images on different scales of the (100) projection of (STO1.2 nm/Co-doped Ba-122 13 nm) × 24 superlattice thin film (Lee et al. 2013a)

doped Ba-122 bilayers and the modulation wavelength is 14 nm in accordance with the design and the XRD measurements. Furthermore, three-unit cell thick STO interlayers have been uniformly grown on the Co-doped Ba-122 layer, as shown in Fig. 13b, which confirm a controllable thickness of the STO interlayer with single unit cell precision and the obtaining of a sharp interface between STO and Co-doped Ba-122. A schematic representation of the structure is illustrated on the right of Fig. 13b, with an evident bonding of the FeAs layer to the SrO layer (Lee et al. 2013a).

In the case of **ferroelectric/paraelectric superlattices,** strong or weak coupling can take place between the ferroelectric layers, depending on the thickness of the layers. For example, the role played by ultrathin STO layers on the control of the domain structure in tricolor SL formed by PT, PZT, and STO has been investigated in Ref (Lemée et al. 2015). The existence of 180° ferroelectric stripe nanodomains, induced by the depolarizing field produced by the STO layers and the polarization rotation resulting from the tensile strains occurring due to the particular combination of single layers, has been observed.

## Engineered Interfaces

Recent successes of the PLD technique in the atomic-scale synthesis of oxide heterostructures have opened a rich field of possibilities to create new states at the interfaces. Examples are interface superconductivity, magnetoelectric coupling, and the quantum Hall effect (Hwang et al. 2012). At the interface between two non-

magnetic insulating perovskites, a magnetic state can be induced. In particular the $ABO_3$ perovskite structure, which can be seen as a stack of alternating AO and $BO_2$ layers when grown in a heterointerface between different materials, introduces polarity discontinuities due to the different valence A and B elements at the interface. Two examples are the LAO/STO and $LaTiO_3$ (LTO)/STO interfaces. An induction of spin states at the interfaces is also expected, besides the charge state modification. A ferromagnetic alignment of the induced electron spins within the Ti-3d conduction is expected for LAO/STO and LTO/STO interfaces. To realize the STO/LAO interface, an STO (001) substrate that was $TiO_2$ terminated was used (Brinkman et al. 2007). A LAO film was grown on this substrate at 850 °C and at different partial oxygen pressures, by PLD, up to 26 unit cells. The intensity oscillations measured by in situ RHEED demonstrated a **layer-by-layer growth** mode. The film was slowly cooled down to ambient temperature in oxygen atmosphere at the same pressure as during the deposition (Brinkman et al. 2007).

In recent years, emergent ferromagnetism has been detected in the $LaAlO_3$/$SrTiO_3$ heterostructure by transport and magnetization studies, due to the presence of mixed valence states of Ti ($Ti^{4+}$ and $Ti^{3+}$). It has been observed that the magnetic $Ti^{3+}$ ion is located mainly at the interface. This effect has been observed in LAO (n)/STO(001) heterostructures samples, prepared by PLD by growing n unit cells of LAO on $TiO_2$-terminated (001) STO substrates (Lee et al. 2013b).

The **conducting interface** between LAO and STO has attracted great attention due to different unexpected properties. For the growth of LAO/STO heterostructures by PLD, the main parameters have been found to be the background gas pressure and the substrate temperature. The oxygen partial pressure $p(O_2)$ is used to control the kinetic energy of the species in the plume. In such a way, in optimized conditions, **atomically smooth surfaces** have been obtained for the grown single crystalline thin films (Choi et al. 2012). Moreover, a control of strain relaxation in film has been achieved, by growing at the beginning a single monolayer of LAO at high $p(O_2)$ pressure. Compared to the low $p(O_2)$ growth, which results into an almost relaxed LAO layer, the insertion of this LAO monolayer prevents the strain relaxation in the LAO film grown afterward at low $p(O_2)$. Moreover, the **interface-engineered heterostructure** displays a more crystalline and sharp interface without **cation intermixing** (Choi et al. 2012).

The authors consider that the shielding layer grown at high $p(O_2)$ prevents the intermixing, thus improving the ability of the thin film to maintain the tensile strain induced by the substrate up to a thickness of at least 50 nm. In addition, they study the crystalline quality by Z-contrast scanning transmission electron microscopy (Z-STEM) and confirm that tuning the $p(O_2)$ at the primary stage of LAO/STO growth is indeed crucial in determining the interface structural quality.

In recent years heterostructures for new interface-based magnetoelectric devices have been investigated. For an optimal tailoring, the understanding of polarization screening and electronic mechanisms is required. These phenomena must be investigated by sophisticated techniques, such as STEM and electron energy-loss spectroscopy (EELS) at a single-unit cell level. Therefore, very high-quality interfaces are required. For example, at the LSMO/BFO interface of the films grown by PLD, a

direct evidence for screening by oxygen vacancies has been obtained (Kim et al. 2014). The oxygen vacancies have been found in the second atomic layer of BFO, due to the different ionic conductivities of the materials. The thin film heterostructures of BFO on (LSMO)/STO have been grown by RHEED-assisted PLD (Kim et al. 2014). BFO films with a thickness of 50 nm have been grown on LSMO layers (5 nm) deposited on $TiO_2$-terminated STO (100) substrates with atomically flat surfaces. A KrF-excimer laser with a fluence of 1.5 J/cm$^2$ and repetition rates of 1 or 2 Hz has been used for the growth of LSMO and BFO layers, respectively. RHEED analysis confirmed the layer-by-layer growth (Kim et al. 2014).

Modern strategies used for obtaining novel multiferroics are based on the modifications in the electronic structure at the interface between ferroelectric and ferromagnetic materials. Due to charge redistribution at the interface, a change in the direction of the ferroelectric polarization may induce a variation of magnetic moment. The inverse effect is also possible. Indeed, both interfacial coupling and ambient temperature interface-induced multiferroicity in Fe/$BaTiO_3$ and Co/$BaTiO_3$ heterostructures have been observed (Valencia et al. 2011). Fe/BTO/LSMO//NGO (001) and Co/BTO/LSMO//NGO (001) have also been investigated. Very thin films of BTO have both spontaneous polarization and magnetization at the interface with Fe or Co, at room temperature. BTO/LSMO heterostructures were grown on (001) NdGaO3 (NGO) substrates, which can induce large compressive strain in BTO films, in order to increase the ferroelectric polarization. The films have been grown by PLD, with a KrF laser with a fluence of 2 J/cm$^2$ and a repetition rate of 1 Hz. It has been found that the magnetization of Fe/BTO and Co/BTO interfaces can be controlled by the ferroelectric polarization direction in BTO (Valencia et al. 2011).

In Ref (Kan et al. 2016) the control of the oxygen coordination environment of the SRO perovskite in a heterostructure with $Ca_{0.5}Sr_{0.5}TiO_3$ (CSTO) grown on a GSO substrate has been demonstrated. The CSTO layer has been grown with a thickness between 1 and 4 monolayers. It has been found that at the SRO/CSTO interface, the Ru-O-Ti angle is dependent on the CSTO layer thickness (Kan et al. 2016). The interface engineering allows therefore to control the structure at the interface (Fig. 14).

The SRO/CSTO/GSO heterostructures were fabricated by epitaxially growing SRO and CSTO layers on (110) GSO substrates by PLD, with excellent interface quality (Kan et al. 2016).

Epitaxial LAO (10 u.c.)/$EuTiO_3$ (2u.c.)/STO **heterostructures** were deposited by RHEED-assisted PLD on $TiO_2$-terminated (001) STO substrates (Stornaiuolo et al. 2016). The simultaneous presence of magnetic interactions, superconductivity, and spin-orbit coupling has been found in this LAO/ETO/STO system.

The synthesis of high-quality heterostructures aims to the growth of atomically sharp interfaces with desired termination sequences. It has been recently shown that the growth oxygen pressure controls the interfacial terminations of $SrRuO_3$/$BaTiO_3$/$SrRuO_3$ (SRO/BTO/SRO) ferroelectric heterostructures (Shin et al. 2017). The heterostructures are grown by PLD with a KrF excimer laser, at the deposition temperature of 700 °C. It has been found that, when the top SRO/BTO interface is grown at high $pO_2$ (~150 mTorr), a mixture of $RuO_2$-BaO and SRO-$TiO_2$

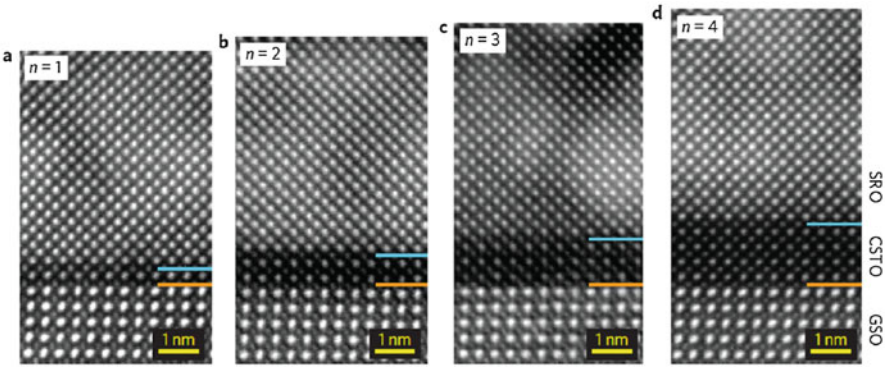


**Fig. 14** HAADF-STEM images of SRO/CSTO-n/GSO heterostructures for the n = 1 (**a**), n = 2 (**b**), n = 3 (**c**), and n = 4 (**d**). The images are taken along the [001] direction of the GSO substrate (Kan et al. 2016)

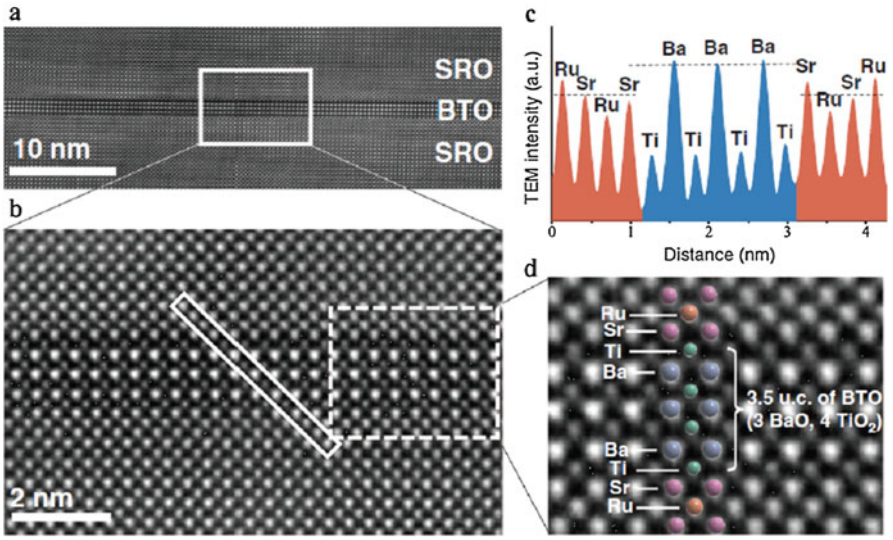


**Fig. 15** (**a**) STEM image of the SRO/BTO/SRO heterostructure; (**b**) STEM image of the region marked by a white box, at larger magnification; (**c**) intensity line profile corresponding to the white bar in (**b**). The profile shows the $TiO_2$ termination at the top and bottom of the BTO layer; (**d**) image of the area inside the white box in (**b**), at higher magnification (Shin et al. 2017)

terminations is obtained. Instead **atomically sharp SRO/BTO interfaces** with uniform SrO-$TiO_2$ termination have been obtained by reducing the $pO_2$ to 5 mTorr. As seen in Fig. 15, high-resolution HAADF images reveal atomically sharp interfaces formed over a lateral range of 40 nm. The BTO layer is uniformly $TiO_2$ terminated for both the top and bottom interfaces. The intensity profile along the solid box in Fig. 15b also confirms the symmetric SrO-$TiO_2$ interface termination

sequences. The thickness of the BTO layer is 3.5 u.c. Using capacitor devices with symmetric and uniform interfacial termination, it is demonstrated for the first time that the FE critical thickness can reach the theoretical limit of 3.5 unit cells (Shin et al. 2017).

Heterostructures with alternate layers of PMN and $PbNbO_3$ have been grown by PLD onto (111) STO substrates using alternate target-timed PLD, for obtaining fully ordered PMN, which is not prepared as bulk material (Shetty et al. 2019).

Self-assembled ferroelectric nanoarrays, of interest for miniaturization of electronic devices like ultrahigh-density FE memories, have been also obtained by PLD (Jiang et al. 2019).

## Photovoltaics and Photocatalysis

In recent years one of the most important research fields is related to the problem of clean energy production with minimum environmental impact. To solve this problem, one of the most popular strategies focuses on the direct conversion of solar energy to electricity. Another important problem to be solved is related to the storage of converted energy in a clean fuel, e.g., hydrogen. For the conversion of solar light energy to electricity, different types of materials (**photovoltaics**) have been developed. The search for materials for **photocatalysis** has also been intensified, focusing on semiconductor materials like oxynitrides. The **oxynitride** materials have bandgap values of about 2 eV which allow to utilize more solar light. They are also stable in water and allow good mobility for the electrons and holes which have been photogenerated.

**Pulsed reactive crossed-beam laser ablation** (PRCLA) was used for the growth of oxynitride $LaTiO_xN_y$ thin films (Pichler et al. 2017). Compared to standard PLD, PRCLA uses a pulsed gas jet of a reactive gas ($NH_3$) injected near the ablation spot at the target surface. $LaTiO_xN_y$ thin films were grown by PRCLA on (001) MgO and (0001) $Al_2O_3$ single crystal substrates coated with epitaxial TiN layers. It has been found that the absorbed photon-to-current conversion efficiency can be tuned by selecting different crystallographic surface orientations. The best results are obtained on films with (001) orientation, where an efficiency about five times higher than for polycrystalline samples have been measured (Pichler et al. 2017).

Metal oxide semiconductors have been investigated as light absorber for all-oxide photovoltaics. $Co_3O_4$ is a p-type semiconductor which has two direct transitions in the visible range, with optical bandgaps of 1.5 eV and 2.2 eV. Thin film heterojunction cells, based on a compact $TiO_2$ layer on which $Co_3O_4$ layer has been deposited by PLD, were investigated as a function of both their layer thicknesses and the $Co_3O_4$ deposition temperature (Kupher et al. 2015). It was found that the deposition temperatures of the $Co_3O_4$ have a strong impact on device performance due to improved crystallinity and morphology of the absorber layer.

In hybrid photovoltaic devices, the most problematic issue is related to the deposition of a highly crystalline metal oxide on the organic material. This has been achieved by employing PLD to deposit highly crystalline ZnO at low

temperatures (200 °C) directly onto the functional organic thin film, poly(3-hexylthiophene) (P3HT), preserving the optical and electronic properties of P3HT (Franklin et al. 2012).

Recently also ferroelectric materials have been investigated for optoelectronic applications (solar cells, electro-optical sensors, etc.) due to presence of a pronounced **ferroelectric photovoltaic effect** in some of these materials. In these materials, the depolarization field associated with the ferroelectric polarization separates the photogenerated electron-hole pairs.

A **microarray** has been constructed based on a **tetragonal $BiFeO_3$** film which has a single domain structure, to avoid the influence of other type of domains which would be present in tetragonal BiFeO3 (Lu et al. 2017). The tetragonal BFO (T-BFO) has also a large remnant polarization, which can induce larger depolarization fields to separate the photogenerated carriers.

T-BFO/LSMO bilayers were epitaxially grown by PLD using a KrF excimer laser (energy density 1.1 J/cm$^2$, repetition rate 8 Hz) in an oxygen pressure of 15 Pa. The LSMO (10 nm) and T-BFO (49 nm) layers were deposited in sequence on the LAO single crystal substrate at 680 °C.

Figure 16 shows the local ferroelectric switching behavior and **photocurrent** image for a 3 × 3 microarray under illumination (light wavelength 365 nm, light intensity 200 mW/cm$^2$). A ± 8 V dc bias has been applied. The 180° phase contrast demonstrates that the polarization direction of the T-BFO domain can be completely reversed by an electric field bias. The dark regions (poled by −8 V) correspond to the upward polarized domains. Vice versa, the bright regions are polarized in the downward direction (Lu et al. 2017). The alternative bright and dark patterns indicate that the ferroelectric polarization reversal in each cell can be well controlled.

Figure 16b shows the photocurrent image of the microarray, measured with **conductive atomic force microscopy** (CAFM) technique. It can be seen that each cell in the microarray exhibits photovoltaic response, which can be reversed by the polarization switching.

Thus, a controllable photovoltaic effect in the epitaxial T-BFO-based heterostructures has been demonstrated at the microscale. The rapid and controllable photovoltaic process opens the way to design novel optoelectronic microdevices (Lu et al. 2017).

## Conducting Thin Films for Electrodes

Recent technology areas such as photovoltaic applications, flat panel displays, etc. require electrodes based on **transparent conductive oxides** (TCO). TCO must show simultaneously high electrical conductivity and high optical transparency in the visible range. Generally, TCO are based on wide-bandgap oxides, which are therefore transparent. Moreover, an adequate amount of suitable doping can ensure metallic behavior. Recently, $Sr_2V_2O_7$ (SVO) films were grown on single crystalline perovskite substrates (001) LSAT and (001) NGO (Mirjolet et al. 2019). Films were grown by PLD using a KrF excimer laser at 5 Hz and a fluence of 2 J/cm$^2$, at 750 °C in argon atmosphere ranging from 0 to 0.3 mbar.

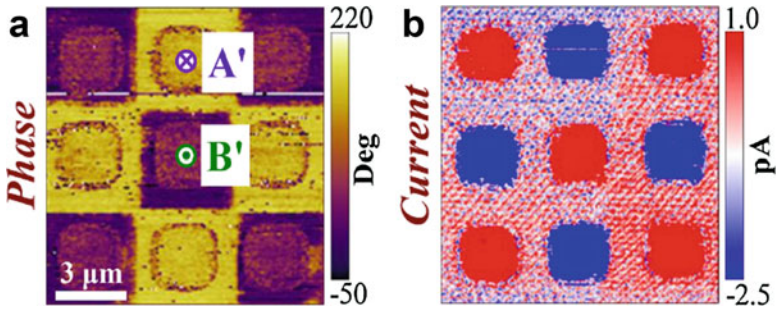


**Fig. 16** (**a**) Local ferroelectric switching for a 3 × 3 microarray of Au/Cr/T-BFO/LSMO (side length of each square electrode is 2.5 μm, and the gap between squares is 1.5 μm), as displayed by ferroelectric phase images recorded by PFM. A′ and B′ represent polarized-down and polarized-up states, respectively; (**b**) photocurrent images scanned by CAFM (Lu et al. 2017)

The growth process has a large effect on the carrier mobility, due to the growth-induced defects in the film. To avoid the effects of energetic plasma particles which can induce defects, SVO films have been grown by PLD in a nonreactive Ar atmosphere, since the nonreactive gas contributes to plasma thermalization and reduces the kinetic energy of the species in the plume and their flux at film surface. SVO films grown under optimal Ar pressure show a very low resistivity (about 30 μOhm cm), thus competing with the record values registered by similar films grown by MBE (Mirjolet et al. 2019). Moreover, the transparency of the films in the visible range has been enhanced, competing with that of the MBE-grown films. These findings indicate that TCO films such as SVO requiring ultralow oxygen pressure deposition conditions can be grown with optimal properties by PLD (Mirjolet et al. 2019).

Other transparent conductive materials have been deposited by PLD: $SrMoO_3$ and $CaMoO_3$ have been grown on STO (001) substrates. A reducing environment of 2.5 $H_2$ in Ar was used at 0.3 mTorr in order to reduce the $Mo^{6+}$ to $Mo^{4+}$ (Stoner et al. 2019)

One of the major drawbacks of solid oxide fuel cells (SOFC) is the high operating temperature (about 800 °C). In recent years many efforts have been directed toward the goal of reducing this temperature. One of the approaches consists in reducing the thickness of the electrolyte to submicron scale. These so-called micro-SOFC are appealing for the use in portable electronics.

In order to follow these advances in the field of SOFC electrolytes, novel electrodes should be developed. The mixed ionic-electronic conducting $La_xSr_{1-x}Co_yFe_{1-y}O_{3-\delta}$ (LSCO) perovskites have been used as SOFC cathode materials. Partially amorphous LSCO thin film cathodes are fabricated using PLD and are integrated in a micro-SOFC with a 3YSZ electrolyte and a Pt anode. The nano-porous columnar microstructure of the LSCO layer provides a large surface area for oxygen incorporation (Evans et al. 2015). The **LSCO cathode** was deposited onto the free standing YSZ/$Si_3N_4$ membranes by PLD at a temperature of 450 °C and oxygen pressure of 0.6 mbar to obtain **nanoporous films** (Evans et al. 2015).

Perovskite BSCF **thin-layer cathodes** for solid-oxide fuel cells were prepared on NiO-YSZ/YSZ composite substrates using PLD and the traditional screen-printing method. The electrochemical properties of the cathode deposited by PLD were superior to those deposited by screen-printing. The maximum power density of the cell made by using PLD was 1.12 W/cm$^2$ compared to 0.45 W/cm$^2$ using the screen-printing method. This enhancement is mainly attributed to the smaller internal resistance within the cathode and the interfacial resistance between the cathode and the electrolyte (Liu et al. 2011).

In the field of batteries, ceramic all-solid-state batteries are preferable due to their high chemical stability and to the possibility of fabrication as thin film devices for portable electronics.

$Li_4Ti_5O_{12}$ lithium titanate **anode thin film**s have been deposited by PLD on $Li_{6.25}Al_{0.25}La_3Zr_2O_{12}$ (LALZO) pellets, demonstrating a good compatibility with the solid garnet electrolyte. These films were deposited with a KrF excimer laser at a frequency of 10 Hz and oxygen pressure of 13 mTorr. $Li_4Ti_5O_{12}$ films were grown on top of LALZO electrolyte pellets for building and testing all-solid Li ion cells. A high stability of the electrode during cycling testing was proven, together with superior properties over other types of electrode material (Pfenninger et al. 2018).

## Perspectives

Pulsed laser deposition has undergone a long way since the first deposition in 1965. A better understanding of the process and instrumental developments, especially of RHEED in PLD, has transformed PLD to a flexible thin film deposition method, which rivals meanwhile MBE for the controlled deposition of high-quality oxide layers. The technological need for devices which require special properties that are based on multilayers, interfaces with control on the atomic level, strained layers, etc. has opened the path for PLD to be transformed from a pure research laboratory-based method to an industrially valuable tool. This transformation is again aided by the instrumental developments from PLD companies, which allow meanwhile large area deposition on wafers of up to 200 mm diameter that matches industrial standards (e.g., Solemates).

**Acknowledgements** One of the authors (M.D.) would like to acknowledge the funding and support received through the Romanian Ministry of Research and Innovation, PN-III-P4-ID-PCCF-2016-0033, 7/2018, as well as the collaboration between SSC Pacific and INFLPR in the frame of CRADA agreement NCRADA-SSCPacific -18-309.

## References

Agar JC, Damodaran AR, Okatan MB et al (2016) Highly mobile ferroelastic domain walls in compositionally graded ferroelectric thin films. Nat Mater 15:549–556

Anisimov SI, Bäuerle D, Luk'yanchuk BS (1993) Gas dynamics and film profiles in pulsed-laser deposition of materials. Phys Rev B 48:12076

Balke N, Choudhury S, Jesse S et al (2009) Deterministic control of ferroelastic switching in multiferroic materials. Nat Nanotechnol 4:868–875

Bäuerle D (2011) Laser processing and chemistry, 3rd edn. Springer, Berlin/Heidelberg/New York

Benckiser E, Haverkort MW, Brück S et al (2011) Orbital reflectometry of oxide heterostructures. Nat Mater 10:189–193

Brinkman A, Huijben M, Van Zalk M et al (2007) Magnetic effects at the interface between non-magnetic oxides. Nat Mater 6:493–496

Choi WS, Rouleau CM, Seo SSA et al (2012) Atomic layer engineering of perovskite oxides for chemically sharp heterointerfaces. Adv Mater 24:6423–6428

Choi E-M, Fix T, Kursumovic A et al (2014) Room temperature ferrimagnetism and ferroelectricity in strained, thin films of $BiFe_{0.5}Mn_{0.5}O_3$. Adv Funt Mater 24:7478–7487

Chrisey DB, Hubler GK (eds) (1994) Pulsed laser deposition of thin films. Wiley, New York

Chu Y-H, Martin LW, Holkomb MB et al (2008) Electric-field control of local ferromagnetism using a magnetoelectric multiferroic. Nat Mater 7:478–482

Craciun F, Verardi P, Dinescu M (2002) Piezoelectric thin films: processing and properties. In: Nalwa HS (ed) Handbook of thin film materials, Vol. 3. Ferroelectric and Dielectric Thin Films. Academic, San Diego, pp 231–309

Damodaran AR, Clarkson JD, Hong Z et al (2017) Phase coexistence and electric-field control of toroidal order in oxide superlattices. Nat Mater 16:1003–1009

Dinescu M, Verardi P (1996) ZnO thin film deposition by laser ablation of Zn target in oxygen reactive atmosphere. Appl Surf Science 106:149–153

Dinescu M, Verardi P, Boulmer-Leborgne C, Gerardi C, Mirenghi L, Sandu V (1998) GaN thin films deposition by laser ablation of liquid Ga target in nitrogen reactive atmosphere. Appl Surf Sci 127–129:559–563

Driza N, Blanco-Canosa S, Bakr M et al (2012) Long-range transfer of electro-phonon coupling in oxide superlattices. Nat Mater 11:675–681

Eason R (2007) Pulsed laser deposition of thin films: applications-led growth of functional materials. Wiley, Hoboken

Eerenstein W, Wiora M, Prieto JL et al (2007) Giant sharp and persistent converse magnetoelectric effects in multiferroic epitaxial heterostructures. Nat Mater 6:348–351

Evans A, Martyczuk J, Stender D et al (2015) Low-temperature micro-solid oxide fuel cells with partially amorphous $La_{0.6}Sr_{0.4}CoO_{3-\delta}$ cathodes. Adv Energy Mater 5:1400747-1-9

Franklin JB, Downing JM, Giuliani F et al (2012) Building on soft foundations: new possibilities for controlling hybrid photovoltaic architectures. Adv Energy Mater 2:528–531

Gajek M, Bibes M, Fusil S et al (2007) Tunnel junctions with multiferroic barriers. Nat Mater 6:296–302

Harrington SA, Zhai J, Denev S et al (2011) Thick lead-free ferroelectric films with high curie temperatures through nanocomposite-induced strain. Nat Nanotechnol 6:491–495

He B, Wang Z (2016) Enhancement of the electrical properties in $BaTiO_3/PbZr_{0.52}Ti_{0.48}O_3$ feroelectric superlattices. ACS Appl Mater Interfaces 8:6736–6742

Hu N, Lu C, Xia Z et al (2015) Multiferroelectricity and magnetoelectric coupling in $TbMnO_3$ thin films. ACS Appl Mater Interfaces 7:26603–26607

Hwang HY, Ywasa Y, Kawasaki M et al (2012) Emergent phenomena at oxide interfaces. Nat Mater 11:103–113

Ion V, Craciun F, Scarisoreanu ND et al (2018) Impact of thickness variation on structural, dielectric and piezoelectric properties of (Ba,Ca)(Ti,Zr)$O_3$ epitaxial thin films. Sci Rep 8:2056-1-9

Jia T, Fan Z, Yao J et al (2018) Multifield control of domains in a room-temperature multiferroic 0.85 $BiTi_{0.1}Fe_{0.8}Mg_{0.1}O_3$-0.15 $CaTiO_3$ thin film. ACS Appl Mater Interfaces 10:20712–20719

Jiang J, Bai ZL, Chen ZH et al (2018) Temporary formation of highly conductive domain walls for non-destructive read-out of ferroelectric domain-wall resistance switching memories. Nat Mater 17:49–55

Jiang J, Yang Q, Zhang Y et al (2019) Self-assembled ferroelectric nanoarray. ACS Appl Mater Interfaces 11:2205–2210

Kan D, Palova L, Anbusathaiah V et al (2010) Universal behavior and electric field induced structural transition in rare-earth-substituted $BiFeO_3$. Adv Funct Mater 20:1108–1115

Kan D, Aso R, Sato R et al (2016) Tuning magnetic anisotropy by interfacially engineering the oxygen coordination environment in a transition metal oxide. Nat Mater 15:432–437

Kim Y-M, Morozovska A, Eliseev E (2014) Direct observation of ferroelectric field effect and vacancy-controlled screening at the $BiFeO_3/La_xSr_{1-x}MnO_3$ interface. Nat Mater 13:1019–1025

Kupher B, Majhi K, Keller DA et al (2015) Thin film $Co_3O_4/TiO_2$ heterojunction solar cells. Adv Energy Mater 5:1401007

Langenberg E, Guzman R, Maurel L et al (2015) Epitaxial stabilization of the perovskite phase in $(Sr_{1-x}Ba_x)MnO_3$ thin films. ACS Appl Mater Interfaces 7:23967–23977

Lee S, Tarantini C, Gao P et al (2013a) Artificially engineered superlattices of pnictide superconductors. Nat Mater 12:392–396

Lee J-S, Xie YW, Sato HK et al (2013b) Titanium dxy ferromagnetism at the $LaAlO_3/SrTiO_3$ interface. Nat Mater 12:703–706

Lemée N, Infante IC, Hubault C et al (2015) Polarization rotation in ferroelectric tricolor $PbTiO_3/SrTiO_3/PbZr_{0.2}Ti_{0.8}O_3$ superlattices. ACS Appl Mater Interfaces 7:19906–19913

Li Z, Guo X, Lu H-B et al (2014) An epitaxial ferroelectric tunnel junction on silicon. Adv Mater 26:7185–7189

Li L, Lu L, Zhang D et al (2016) Direct observation of magnetic field induced ferroelectric domain evolution in self-assembled quasi (0-3) $BiFeO_3$-$CoFe_2O_4$ thin films. ACS Appl Mater Interfaces 8:442–448

Liu B, Chen X, Dong Y et al (2011) A high-performance, nanostructured $Ba_{0.5}Sr_{0.5}Co_{0.8}Fe_{0.2}O_{3-\delta}$ cathode for solid-oxide fuel cells. Adv Energy Mater 1:343–346

Lorazo P, Lewis LJ, Meunier M (2006) Thermodynamic pathways to melting, ablation, and solidification in absorbing solids under pulsed laser irradiation. Phys Rev B 73:134108

Lu Z, Li P, Wan J-G et al (2017) Controllable photovoltaic effect of microarray derived from epitaxial tetragonal $BiFeO_3$ films. ACS Appl Mater Interfaces 9:27284–27289

Lyu J, Estandia S, Gazquez J et al (2018) Control of polar orientation and lattice strain in epitaxial $BaTiO_3$ films on silicon. ACS Appl Mater Interfaces 10:25529–25535

McGilly LJ, Yudin P, Feigl L et al (2015) Controlling domain wall motion in ferroelectric thin films. Nat Nanotechnol 10:145–150

Miotello A, Kelly R (1995) Critical assessment of thermal models for laser sputtering at high fluences. Appl Phys Lett 67:3535

Mirjolet M, Sanchez F, Fontcuberta J (2019) High carrier mobility, electrical conductivity and optical transmittance in epitaxial $SrVO_3$ thin films. Adv Funct Mater 29:1808432-1-7

Nguyen MD, Houwman PE, Dekkers M et al (2017a) PZT films with vertically aligned columnar grains with strongly enhanced piezoelectric response. ACS Appl Mater Interfaces 9:9849–9861

Nguyen MD, Houwman EP, Yuan H et al (2017b) Controlling piezoelectric response in $Pb(Zr_{0.52}Ti_{0.48})O_3$ films through deposition conditions and nanosheet buffer layers on glass. ACS Appl Mater Interfaces 9:35947–35957

Ojeda-G-P A, Döbeli M, Lippert T (2018) Influence of plume properties on thin film composition in pulsed laser deposition. Adv Mater Interfaces 5:1701062

Ossi PM (2018) Advances in the application of lasers in materials science, Springer series in materials science, vol 274. Springer Nature Switzerland, Cham

Pandya S, Wilbur J, Kim J et al (2018) Pyroelectric energy conversion with large energy and power density in relaxor ferroelectric thin films. Nat Mater 17:432–438

Pfenninger R, Afyon S, Garbayo I et al (2018) Lithium titanate anode thin films for Li-ion solid state battery based on garnets. Adv Funct Mater 28:1800879-1-8

Pichler M, Si W, Haydous F et al (2017) $LaTiO_xN_y$ thin film model systems for photocatalytic water splitting: physicochemical evolution of the solid-liquid interface and the role of the crystallographic orientation. Adv Func Mater 27:1605690

Puretzky AA, Merkulov IA, Rouleau CM, Eres G, Geohegan DB (2014) Revealing the surface and bulk regimes of isothermal graphene nucleation and growth on Ni with in situ kinetic measurements and modeling. Carbon 79:256–264

Sando D, Agbelele A, Rahmedov D et al (2013) Crafting the magnonic and spintronic response of $BiFeO_3$ films by epitaxial strain. Nat Mater 12:641–646

Scarisoreanu ND, Craciun F, Moldovan A (2015) High permittivity (1-x)$Ba(Zr_{0.2}Ti_{0.8})O_3$-x $(Ba_{0.7}Ca_{0.3})TiO_3$ (x = 0.45) epitaxial thin films with nanoscale phase fluctuations. ACS Appl Mater Interfaces 7:23984–23992

Scarisoreanu ND, Craciun F, Birjega R et al (2016) Joining chemical pressure and epitaxial strain to yield Y-doped $BiFeO_3$ thin films with high dielectric response. Sci Rep 6:25535-1-13

Scarisoreanu ND, Craciun F, Ion V, Birjega R, Bercea A, Dinca V, Dinescu M, Sima LE, Icreverzi M, Roseanu A, Gruionu L, Gruionu G (2017) Lead-free piezoelectric $(Ba,Ca)(Zr,Ti)O_3$ thin films for biocompatible and flexible devices. ACS Appl Mater Interfaces 9:266–278

Shetty S, Damodaran A, Wang K (2019) Relaxor behavior in ordered lead magnesium niobate $(PbMg_{1/3}Nb_{2/3}O_3)$ thin films. Adv Funct Mater 29:1804258-1-9

Shin JS, Kim Y, Kang S-J et al (2017) Interface control of ferroelectricity in an $SrRuO_3/BaTiO_3/SrRuO_3$ capacitor and its critical thickness. Adv Mater 29:1602795-1-6

Singh RK, Narayan J (1990) Pulsed-laser evaporation technique for deposition of thin films: physics and theoretical model. Phys Rev B 41:8843

Smith M, Turner AF (1965) Vacuum deposited thin films using a ruby laser. Appl Opt 4:147–148

Stoner LA, Murgatroyd PAE, O'Sullivan M et al (2019) Chemical control of correlated metals as transparent conductors. Adv Funct Mater 29:1808609-1-7

Stornaiuolo D, Cantoni C, De Luca GM et al (2016) Tunable spin polarization and superconductivity in engineered oxide interfaces. Nat Mater 15:278–283

Studenikin SA, Golego N, Cocivera M (1998) Optical and electrical properties of undoped ZnO films grown by spray pyrolysis of zinc nitrate solution. J Appl Phys 83:2104

Tyunina M, Yao L, Plekh M et al (2013) Epitaxial ferroelectric heterostructures with nanocolumn-enhanced dynamic properties. Adv Funct Mater 23:467–474

Valencia S, Crassous A, Bocher L et al (2011) Interface-induced room-temperature multiferroicity in $BaTiO_3$. Nat Mater 10:753–758

Vasudevan RK, Morozovska AN, Eliseev EA et al (2012) Domain wall geometry controls conduction in ferroelectrics. Nano Lett 12:5524–5531

Verardi P, Dinescu M, Andrei A (1996) Characterization of ZnO thin films deposited by laser ablation in reactive atmosphere. Appl Surf Sci 96-98:827–830

Verardi P, Nastase N, Gherasim C, Ghica C, Dinescu M, Dinu R, Flueraru C (1999) Scanning force microscopy and electron microscopy studies of pulsed laser deposited ZnO thin films: application to the bulk acoustic waves (BAW) devices. J Crystal Growth 197:523–528

Wei Y, Nukala P, Salverda M et al (2018) A rhombohedral ferroelectric phase in epitaxially strained $Hf_{0.5}Zr_{0.5}O_2$ thin films. Nat Mater 17:1095–1100

Wen Z, Li C, Wu D et al (2013) Ferroelectric-field-effect-enhanced electroresistance in metal/ferroelectric/semiconductor tunnel junctions. Nat Mater 12:617–621

Wu SM, Cybart SA, Yu P et al (2010) Reversible electric control of exchange bias in a multiferroic field-effect device. Nat Mater 9:756–761

Xu R, Liu S, Grinberg I et al (2015) Ferroelectric polarization reversal via successive ferroelastic transitions. Nat Mater 14:79–86

Yin YW, Burton JD, Kim Y-M et al (2013) Enhanced tunneling electroresistance effect due to a ferroelectrically induced phase transition at a magnetic complex oxide interface. Nat Mater 12:397–402

Zhu XN, Gao TT, Xu X et al (2016) Piezoelectric and dielectric properties of multilayered $BaTiO_3/(Ba,Ca)TiO_3/CaTiO_3$ thin films. ACS Appl Mater Interfaces 8:22309–22315